NACA TN 2114

NATIONAL ADVISORY COMMITTEE FOR AERONAUTICS

TECHNICAL NOTE 2114

THEORETICAL LIFT AND DAMPING IN ROLL OF THIN WINGS WITH ARBITRARY SWEEP AND TAPER AT SUPERSONIC SPEEDS

SUPERSONIC LEADING AND TRAILING EDGES

By Sidney M. Harmon and Isabella Jeffreys

Langley Aeronautical Laboratory
Langley Air Force Base, Va.

PRINCETON UNIVERSITY
THE JAMES FORRESTAL
RESEARCH CENTER
LIBRARY

Washington
May 1950

NATIONAL ADVISORY COMMITTEE FOR AERONAUTICS

TECHNICAL NOTE 2114

THEORETICAL LIFT AND DAMPING IN ROLL OF THIN WINGS WITH ARBITRARY SWEEP AND TAPER AT SUPERSONIC SPEEDS

SUPERSONIC LEADING AND TRAILING EDGES

By Sidney M. Harmon and Isabella Jeffreys

SUMMARY

Generalized expressions are obtained by means of the linearized theory for the surface velocity potentials and the surface-pressure distributions due to lift and roll, the lift-curve slope, and the damping-in-roll derivative for a series of thin wings. The results are applicable to wings of arbitrary taper ratio in which the leading edge is sweptback, whereas the trailing edge is either sweptback or swept-forward (including zero sweep angles), and the tips are unyawed with respect to the free-stream direction. The range of speeds covered is such that the components of the stream velocity normal to the leading and trailing edges are supersonic. A further restriction is that the foremost Mach line from either tip may not intersect the remote half-wing. The configurations for which the results for the stability derivatives are applicable may be extended by means of the reversibility theorem. These additional configurations include cases in which the foremost Mach line from either tip intersects the remote half-wing, provided the Mach line from the leading edge of the center section intersects the trailing edge, and also wings which have sweptforward leading edges.

The results of the investigation are presented in the form of generalized design curves for rapid estimation of the derivatives.

INTRODUCTION

The lift and damping in roll as obtained from the linearized theory of supersonic flow have been reported for various ranges of supersonic speeds for thin wings having particular plan forms (for example, see references 1 to 7). In reference 7, generalized curves are presented for the lift-curve slope C_{L_α} and the damping-in-roll C_{l_p}

for a particular family of tapered sweptback wings for a range of supersonic speeds for which the wing lies within the Mach cone emanating from the leading edge of the center section but lies ahead of the Mach cone emanating from any point along the trailing edge (subsonic leading edge and supersonic trailing edge).

In the present paper, the range of speeds which is considered in reference 7 is extended and data are obtained for cases in which a portion of the wing always lies ahead of the Mach cone emanating from any point along the leading edge (supersonic leading edge) although the trailing edge is still supersonic. The wings considered have an arbitrary taper ratio, leading and trailing edges that are each swept at a constant angle (including zero sweep angles), and tips that are unyawed with respect to the free-stream direction. The results of the analysis for wings with sweptback leading edges and either sweptback or sweptforward trailing edges are given in the form of generalized equations for the surface velocity potential and for the surface-pressure distribution for the wing at an angle of attack and in a steady rolling motion. Generalized equations are also given for these wings for the derivatives C_{L_α} and C_{l_p}. A series of generalized curves is presented, from which rapid estimations of C_{L_α} and C_{l_p} can be made for given values of aspect ratio, taper ratio, Mach number, and leading-edge sweep. Some illustrative variations of the derivatives with these parameters are also given.

As shown in references 8 and 9, the theorem of reversibility applies to the derivatives C_{L_α} and C_{l_p} for the wings considered in this paper $\left(\text{see also reference 10 for } C_{L_\alpha}\right)$. Consequently, the results for these derivatives, which are presented for wings with sweptback leading edges, apply as well to the corresponding sweptforward wings obtained by reversing the flight direction. In order to present a complete and systematic analysis, some data pertaining to the present calculations which have been given in other papers have been incorporated herein.

SYMBOLS

x,y,z rectangular coordinates with origin at leading edge of center section (figs. 1 and 3(a))

x_a,y_a indicates a transformation of origin of x- and y-axes from leading edge of center section to leading edge of tip section $\left(x_a = x - \frac{h}{m};\ y_a = y - h \text{ on right half-wing}\right)$

$\nu = \frac{y}{mx}$

$\nu_a = \frac{y_a}{mx_a}$

V	undisturbed flight velocity
M	free-stream Mach number
$B = \sqrt{M^2 - 1}$	
α	wing angle of attack
p	angular velocity about x-axis, radians
μ	Mach angle $\left(\sin^{-1} \frac{1}{M} \text{ or } \cot^{-1} B\right)$
Λ	sweep of wing leading edge, positive for sweepback
Λ_{TE}	sweep of wing trailing edge, positive for sweepback
$m = \cot \Lambda$	
h	wing semispan
b	wing span
c	chord at arbitrary spanwise position
c_r	root chord
c_t	tip chord
λ	taper ratio (c_t/c_r)
S	wing area $\left(\frac{bc_r(1 + \lambda)}{2}\right)$
A	aspect ratio $\left(\frac{2b}{c_r(1 + \lambda)}\right)$

$$k = \frac{\cot \Lambda_{TE}}{\cot \Lambda} = \frac{BA(1 + \lambda)}{BA(1 + \lambda) - 4Bm(1 - \lambda)}$$

$A' = BA$

$m' = Bm$

$J = A'(1 + \lambda)$

ρ free-stream mass density of air

ϕ disturbance-velocity potential on upper surface of airfoil

$\phi_x = \frac{\partial \phi}{\partial x}$

ΔP pressure difference between lower and upper surfaces of airfoil, positive in direction of lift

ΔC_p nondimensional coefficient expressing ratio of pressure difference between lower and upper surfaces of airfoil to free-stream dynamic pressure $\left(\frac{\Delta P}{\frac{1}{2}\rho V^2}\right)$

ΔC_{p_t} contribution of wing cut-off at tip to ΔC_p; used with subscripts α and p to refer to angle of attack and steady rolling motion, respectively

X,Y,Z forces parallel to x-, y-, and z-axes, respectively

L lift

L' rolling moment

C_L lift coefficient $\left(\frac{L}{\frac{1}{2}\rho V^2 S}\right)$

C_l rolling-moment coefficient $\left(\frac{L'}{\frac{1}{2}\rho V^2 Sb}\right)$

$C_{L_\alpha} = \left(\frac{\partial C_L}{\partial \alpha}\right)_{\alpha \to 0}$

$C_{l_p} = \left(\frac{\partial C_l}{\partial \frac{pb}{2V}}\right)_{\frac{pb}{2V} \to 0}$

Subscripts:

R refers to reverse of a given wing, obtained by reversing flow direction

TE refers to trailing edge

ANALYSIS

Scope

The analysis is limited to wings of vanishingly small thickness that have zero camber. The results are valid only for a range of supersonic speeds in which the components of the free-stream velocity normal to the leading and trailing edges are supersonic. These conditions are now commonly expressed by the term "supersonic leading and trailing edges". The wing configurations considered in the analysis are defined by the information and sketches given in figures 1 and 2. All the data obtained in the analysis for the velocity potential and pressure distributions and for the derivatives C_{L_α} and C_{l_p} are applicable to the wings of the type shown in figure 1. These wings have sweptback leading edges, although the trailing edges may be either sweptback or sweptforward. A further restriction is that the Mach waves from either tip may not intersect the remote half-wing.

It is indicated subsequently that, although the data for the velocity potential and pressure distributions are applicable only to wings of the type shown in figure 1, the results for C_{L_α} and C_{l_p} may be applied also to an additional series of wing configurations by use of the theorem of reversibility. This additional series of wings is indicated in figure 2. The wings in the figure have supersonic leading and trailing edges. In figure 2(a), the leading edge is sweptforward. The configuration shown in figure 2(b) represents an increase in the range of applicability for BA over that indicated in figure 1. This increase in the BA range, by means of the theorem of reversibility, is discussed in the section entitled "Results and Discussion" and corresponds to the allowance that the Mach waves from a tip may intersect the remote half-wing, provided the Mach line from the leading edge of the center section intersects the trailing edge of the wing.

The orientation of the wing with respect to a body system of coordinate axes used in the analysis is indicated in figure 3(a). The surface velocity potentials, the pressure distributions, and the stability derivatives are derived with respect to this system. Figure 3(b) shows the wing oriented with respect to the stability-axes system. A transformation of the body system of axes to the stability system of axes

(references 11 and 5) indicates that to the first order in α, the derivatives C_{L_α} and C_{l_p} have the same value in the stability system as they do in the body-axes system shown in figure 3(a).

Method

Basic considerations.- The evaluation of the derivatives C_{L_α} and C_{l_p} involves the integration over the wing of the disturbance pressures caused by an angle of attack α and a steady rolling angular velocity p, respectively. In the treatment of small disturbances, such as are considered in this analysis, the disturbance pressures may be determined from the well-known relationship

$$\Delta C_p = \frac{\Delta P}{\frac{1}{2}\rho V^2} = \frac{2\rho V \phi_x}{\frac{1}{2}\rho V^2} = \frac{4}{V}\phi_x \tag{1}$$

Derivation of ϕ and ΔC_p distributions.- The potential function ϕ must be determined so as to satisfy the linearized partial differential equation of the flow and the boundary conditions that are associated with the wing in its prescribed motion.

The methods for deriving the pressure distribution for lifting swept wings of finite aspect ratio of the type considered herein are extensively treated in the literature (for example, references 1, 2, 4, and 12 to 15). In the present analysis, it was found convenient to obtain the surface-potential function and the pressure distribution on the wing by means of the method and data presented in references 14, 15, or 16.

Expressions for ϕ and ΔC_p distributions.- For purposes of obtaining generalized expressions for the surface velocity potential and pressure distributions, a general wing of the type considered in this analysis is conveniently divided into five individual regions. These regions are indicated in figure 4 and are defined by means of Mach forecone boundaries which yield regions in which all points are influenced by a particular type of disturbance. Thus all points in region 1 are influenced by a disturbance which is identical to that induced by an infinitely long oblique wing. Points in region 2 are influenced by a disturbance which is identical to that induced by a triangular wing. Points in region 3 experience two types of disturbances; one of these is the same type as that in region 1 and the other results from the effect of the wing cut-off at the tip which is hereinafter denoted as the tip effect. Points in region 4 experience disturbances which include all types associated with regions 1, 2, and 3. Consequently, the formula

for ϕ or ΔC_p in region 4 expresses the effects of all the disturbances experienced in regions 1, 2, and 3. When the ϕ or ΔC_p expression as determined for region 4 is used for any of the regions 1, 2, or 3, certain terms become imaginary. These imaginary terms indicate the condition that a disturbance type associated with region 4 vanishes in the other regions 1, 2, or 3. The foregoing facts show that the expression for ϕ or ΔC_p in any of the regions 1, 2, 3, or 4 is found simply as the real part of ϕ or ΔC_p as determined for region 4. Points in region 5 are actually influenced by all the disturbances which affect region 4, together with a new disturbance which arises from the tip effect associated with region 2. However, if the effective forezone of influence is drawn for points in region 5, that is, if the external field is canceled by the appropriate area on the wing surface, the effect of the adjacent half-wing disturbance is seen to be completely canceled by the tip effect arising from region 1. The real part of the expression for ϕ or ΔC_p, as determined for region 5, consequently does not yield the corresponding formulas for the other regions.

The formulas for ϕ and ΔC_p for the five regions for a general wing of the type considered in this analysis are summarized in tables I and II for the cases of angle of attack and rolling, respectively. It is significant to note in table II that in regions 1 to 4 the pressure distributions caused by an angle of attack are conical ($f(\nu)$ or $f(\nu_a)$) and those caused by steady rolling are quasi-conical ($xf(\nu)$ or $x_a f(\nu_a)$). Examples of the pressure distribution in the chordwise and spanwise directions for the cases of angle of attack and rolling are given in figures 5 and 6, respectively.

Derivation of formulas for C_{L_α} and C_{l_p}.- The derivatives C_{L_α} and C_{l_p} are basically obtained by integrating over the wing the quantities $\Delta C_p(x,y)$ and $\Delta C_p(x,y)$ times its moment arm, respectively. Thus

$$C_{L_\alpha} = \frac{1}{S\alpha}\iint_S \Delta C_p \, dx \, dy \tag{2}$$

$$C_{l_p} = \frac{1}{Sb \; pb/2V}\iint_S \Delta C_p y \, dx \, dy \tag{3}$$

where $\Delta C_p = \frac{4}{V}\phi_x$ and ϕ_x for the angle of attack and rolling cases are linear functions of α and p, respectively.

The conical form of ΔC_p for C_{L_α} $(f(\nu)$ or $f(\nu_a))$ and the quasi-conical form of ΔC_p for C_{l_p} $(xf(\nu)$ or $x_a f(\nu_a))$, as indicated in table II for regions 1 to 4, make it convenient to employ a polar integration procedure. In this polar integration procedure, the variable of integration y or y_a is replaced by the variable ν or ν_a, respectively, and the integrations in equations (2) and (3) are conveniently performed first with respect to x and then with respect to ν or ν_a. In some cases in the present analysis, it was found convenient to utilize the potential function ϕ to obtain the derivatives C_{L_α} and C_{l_p}. Thus, for a lifting wing, the linearized, thin-airfoil theory yields a potential function ϕ which is antisymmetrical with respect to the xy-plane $(z = 0)$. Furthermore, ϕ is continuous for z = Constant (either $z \longrightarrow +0$ or $z \longrightarrow -0$). Consequently, ϕ is zero at the wing leading edge. Then, because ϕ_x is continuous on the wing, there results

$$\int_{L.E.}^{T.E.} \Delta C_p \, dx = \frac{4}{V} \int_{L.E.}^{T.E.} \phi_x \, dx = \frac{4}{V} \phi_{TE} \tag{4}$$

The total lift per unit span along any wing section, consequently, is proportional to the value of the potential at the trailing edge. Similarly, the rolling moment contributed by any wing section is proportional to the product of the potential at the trailing edge and its moment arm. Thus the derivatives are

$$C_{L_\alpha} = \frac{4}{VS\alpha} \int_{y_{TE}} \phi_{TE} \, dy \tag{5}$$

and

$$C_{l_p} = \frac{4}{VSb \; pb/2V} \int_{y_{TE}} \phi_{TE} y \, dy \tag{6}$$

where the integrals are evaluated along the wing trailing edge. For cases in which the derivatives were expressed in the form of equations (5) or (6), the potential ϕ_{TE} was obtained from table I by specifying x and y or x_a and y_a for conditions along the wing trailing edge.

RESULTS AND DISCUSSION

Formulas for C_{L_α} and C_{l_p}

The formulas for C_{L_α} and C_{l_p} are summarized in the appendix. It may be found from an examination of table II that the pressure distributions are in general markedly different for the cases where the Mach line from the leading edge of the center section intersects the wing tip and where this Mach line intersects the wing trailing edge. In order to determine the derivatives C_{L_α} and C_{l_p}, however, it is sufficient to integrate the forces or moments on the wing as determined for the case in which the Mach line intersects the wing tip. The real parts of the resulting expressions then also yield the corresponding derivatives C_{L_α} and C_{l_p} for the case in which the Mach line intersects the wing trailing edge. This fact results from the inherent rule of supersonic flows that any disturbance cannot propagate ahead of the Mach aftercone. Then the first case (Mach line cutting tip) may be converted to the second case (Mach line cutting trailing edge) by cutting off an appropriate rear portion of the wing. This conversion does not alter in any way the original pressure distribution over the new wing. Thus, if the expressions for C_{L_α} and C_{l_p} as determined for the first case are now applied to the second case, certain terms which arise from disturbances peculiar to the first case become imaginary, and the remaining terms that are real yield the corresponding expressions for C_{L_α} and C_{l_p} for the second case.

Charts for BC_{L_α} and BC_{l_p}

The results of computations for the derivatives C_{L_α} and C_{l_p} are presented in figures 7 and 8, respectively. The data are shown for values of taper ratio λ from 0 to 1.0 for values of aspect-ratio parameter BA from 2 to 20. The range of sweep angles covers values for sweep-angle parameter $B \cot \Lambda$ from 1 to ∞.

For constant B, that is, constant M, the curves in figures 7 and 8 indicate directly the variation of C_{L_α} and C_{l_p}, respectively, with sweep for constant values of A and λ. In this case the curves for increasing values of $B \cot \Lambda$ correspond to decreasing angles of sweepback for both the leading and trailing edges. Some specific variations of the derivatives C_{L_α} and C_{l_p} with Mach number, aspect ratio, sweep angle, and taper ratio are shown in figures 9 and 10. The wing parameters represented in the figures include configurations with

supersonic and subsonic leading edges and supersonic trailing edges. The results for the supersonic leading edges were obtained from figures 7 and 8 of this paper and those for the subsonic leading edges were obtained from reference 7. (Note that application of the reversibility theorem to the results of reference 7 for wings with subsonic leading edges and supersonic trailing edges will yield corresponding results for wings with supersonic leading edges and subsonic trailing edges.)

The data in these figures show that the manner in which C_{L_α} and C_{l_p} vary with many of the factors depends to an important extent on the value of the aspect-ratio parameter BA. Figures 7 and 8 show, for constant Mach number, that when BA is less than approximately 3, the magnitudes of C_{L_α} and C_{l_p} tend to increase with decreasing sweep angle; however, when BA is greater than approximately 3, the magnitudes of these derivatives tend to increase with increasing sweep angle. This general trend for values of BA greater than approximately 3 becomes more pronounced as BA is increased. These data indicate also that for values of B cot Λ greater than approximately 3, the sweep of the leading and trailing edges for constant BA and λ have a very small effect on BC_{L_α} or BC_{l_p}.

The foregoing trends may be explained by the relation of the Mach aftercone which emanates from the leading edge of the center section to the wing tip. This relationship has an important effect on the contribution of the wing tip region to the derivatives C_{L_α} and C_{l_p}. If the quantity

$$B \cot \Lambda < \frac{AB(1 + \lambda)}{AB(1 + \lambda) - 4\lambda}$$

then the Mach line from the leading edge of the center section cuts the wing tip. This condition yields region 5 in figure 4. If the effective forezone of influence is drawn for points in region 5, that is, if the external field is canceled by the appropriate area on the wing surface, it is seen that the pressure distributions in this region for both angle of attack and rolling are determined only by the sources in a strip along the leading edge of the remote half-wing. Because these sources generally are at a comparatively large distance from region 5, the contribution of region 5 to C_{L_α} is comparatively small (see fig. 5). In the case of rolling, these sources at the leading edge of the remote half-wing actually contribute negative damping to region 5 because these sources have the reverse sign from those on the adjacent half-wing (see fig. 6). For a given value of B cot Λ, from geometric considerations, this influence of region 5 in reducing the magnitudes of C_{L_α} and C_{l_p} decreases as the value of BA increases.

Similarly, from geometric considerations, the influence of region 5 in reducing the magnitudes of C_{L_α} and C_{l_p} increases as the value of the taper ratio λ increases. This factor contributes to an important extent to the trend that the maximum values of C_{L_α} and C_{l_p} occur at progressively lower values of λ as BA decreases (see figs. 9 and 10).

Extensions of C_{L_α} and C_{l_p} Results by Reversibility Theorem

Increased range for BA.- The direct application of the formulas in the appendix is limited by the restrictions that the leading edge is sweptback and is supersonic, that the trailing edge is supersonic, and that the foremost Mach line from either tip does not intersect the remote half-wing. As noted in the introduction, however, the reversibility theorem for C_{L_α} and C_{l_p} is applicable for all the plan forms used in the derivation of these formulas. In this connection, wing plan forms of the type shown in figure 2(b) require special attention. In these cases, the foremost Mach line from either tip intersects the remote half-wing, that is,

$$BA < \frac{4B \cot \Lambda}{(1 + \lambda)(1 + B \cot \Lambda)}$$

therefore these conditions are outside the validity of the formulas in the appendix. It can be shown, however, that if this reduced-aspect-ratio parameter is accompanied by the condition that the foremost Mach line from the center section intersects the trailing edge, that is

$$BA \geqq \frac{4\lambda B \cot \Lambda}{(1 + \lambda)(B \cot \Lambda - 1)}$$

the reverse of the wings shown in figure 2(b) will meet all the conditions for the validity of the formulas in the appendix. Thus the values for C_{L_α} and C_{l_p} for wings of the type shown in figure 2(b) can be calculated from the formulas in the appendix by using the wing parameters for the reverse of the given wing, and applying the calculated result to the given wing. If the subscript R refers to the reverse of the given wing, the parameters to be used in the formulas are related in the following manner:

$$\begin{aligned} BA_R &= BA \\ \lambda_R &= \lambda \\ Bm_R &= -Bmk \\ k_R &= \frac{1}{k} \end{aligned} \tag{7}$$

Wings with sweptforward leading edges.- The results for BC_{L_α} and BC_{l_p} which are shown in figures 7 and 8 for wings in which the leading edges are swept back (positive values for $B \cot \Lambda$) can be applied to wings with sweptforward leading edges (negative values for $B \cot \Lambda$) by use of the reversibility theorem. (See fig. 2 for applicable wing configurations.) Thus, suppose the sweep-angle parameter is expressed as $B \cot \Lambda$ where this quantity is negative and where the reverse of the given wing meets all the conditions for the validity of the data in figures 7 and 8 as indicated in figure 1; the values for BC_{L_α} and BC_{l_p} for the given wing are then obtained from figures 7 and 8, respectively, by choosing a wing for which the relationships expressed by equation (7) apply. Thus

$$B \cot \Lambda_R = \frac{B^2 A \cot \Lambda(1 + \lambda)}{4B \cot \Lambda(1 - \lambda) - BA(1 + \lambda)}$$

$$BA_R = BA$$

and

$$\lambda_R = \lambda$$

where the subscript R refers to the parameters to be used in figures 7 and 8.

An illustrative comparison of BC_{L_α} and BC_{l_p} for wings with sweptback and sweptforward leading edges is given in figures 11 and 12, respectively. The data in these figures are presented for a taper ratio of 0.5, for values of BA of 2, 4, and 10, and for a range of $B \cot \Lambda$ from -5 to 5. The wing parameters represented in the figures include configurations with supersonic and subsonic leading and trailing edges.

The results for the sweptback leading edges were obtained from figures 7 and 8 of this paper for the supersonic leading and trailing edges and from reference 7 for the subsonic leading edges and subsonic and supersonic trailing edges. In the case of the subsonic trailing edges, the results from reference 7 have a limited significance in that they represent an upper limit for the true values of the derivatives. The limited signifance of the results for the subsonic trailing edges is indicated in figures 11 and 12 by means of the dashed portions of the curves.

The results for the sweptforward wings were obtained by use of the reversibility theorem. In this connection, it should be noted that the

reversibility theorem for C_{L_α} and C_{l_p} is applicable even for subsonic leading and trailing edges (reference 9).

The comparison for the wings with sweptback and sweptforward leading edges in figures 11 and 12 indicates that the curves for BC_{L_α} and BC_{l_p} for $\lambda = 0.5$ are, in general, very nearly symmetrical with respect to the ordinate axis. The significance of the symmetry of the curves is better visualized when it is noted that, for a specified A, λ, and Λ, if the sweep angle of the leading edge is reversed in sign to $-\Lambda$, there is also an alteration in the sweep angle of the trailing edge, the magnitude of which is dependent on the various wing parameters. Consequently, the near symmetry of the BC_{L_α} and BC_{l_p} curves in figures 11 and 12 for $\lambda = 0.5$ indicates that for a given A and Λ, if Λ is reversed in sign, the values for the derivatives C_{L_α} and C_{l_p} are, in general, only slightly changed even though the sweep angles of the trailing edges of the two wings may be markedly different. For the case of an untapered wing, the theorem of reversibility indicates that C_{L_α} and C_{l_p} are unchanged by reversing the signs of Λ and Λ_{TE}, that is, the corresponding curves in figures 11 and 12 would be identically symmetrical with respect to the axis of ordinates for all values of BA.

CONCLUDING REMARKS

Generalized expressions have been obtained by means of the linearized theory for the surface velocity potentials and the surface-pressure distributions due to lift and roll, the lift-curve slope, and the damping-in-roll derivative for a series of thin wings. The results are applicable to wings of arbitrary taper ratio in which the leading edge is sweptback, whereas the trailing edge is either sweptback or sweptforward (including zero sweep angles), and the tips are unyawed with respect to the free-stream direction. The range of speeds covered was such that the components of the stream velocity normal to the leading and trailing edges were supersonic. A further restriction is that the foremost Mach line from either tip may not intersect the remote half-wing.

The configurations for which the results for the stability derivatives are applicable may be extended by means of the reversibility theorem. These additional configurations include cases in which the foremost Mach line from either tip intersects the remote half-wing, provided the Mach line from the leading edge of the center section intersects the trailing edge, and also wings which have sweptforward

leading edges. The results of the investigation were presented in the form of generalized design curves for rapid estimation of the derivatives.

A significant result of the investigation was that for constant Mach number when $A\sqrt{M^2 - 1}$ (where A is aspect ratio and M is Mach number) was less than approximately 3, the magnitudes of the lift-curve slope C_{L_α} and the damping-in-roll derivative C_{l_p} tended to increase with decreasing sweep angles; however, when $A\sqrt{M^2 - 1}$ was greater than approximately 3, the magnitudes of these derivatives tended to increase with increasing sweep angle.

Langley Aeronautical Laboratory
National Advisory Committee for Aeronautics
Langley Air Force Base, Va., February 23, 1950

APPENDIX

SUMMARY OF FORMULAS FOR C_{L_α} AND C_{l_p}

The following formulas for C_{L_α} and C_{l_p} refer to wings which have an arbitrary taper ratio, leading and trailing edges that are each swept at a constant angle (including zero sweep angles), and tips that are unyawed with respect to the free-stream direction. These configurations are limited by the conditions (see fig. 1)

$$B \cot \Lambda \geqq 1$$

$$\left| B \cot \Lambda_{TE} \right| \geqq 1$$

and

$$BA \geqq \frac{4B \cot \Lambda}{(1 + \lambda)(1 + B \cot \Lambda)}$$

Note that the trailing edges may be either sweptforward or sweptback. In the formulas, care must be used to preserve the correct sign of the terms involving radicals. For example, if $a < 0$ and $b < 0$, then

$$\sqrt{ab} = \sqrt{(-1)^2 \left|a\right|\left|b\right|} = -\sqrt{\left|a\right|\left|b\right|}$$

It may be of interest to mention that in computing with the formulas, it was found that if seven significant figures were used, reliable results were obtained.

Formulas for C_{L_α}

If the Mach line is coincident with the leading edge, that is, $B \cot \Lambda = 1$, there result:

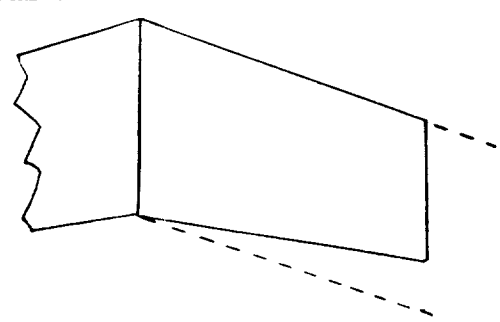

For tapered wings:

$$C_{L_\alpha} = \frac{2A'}{\pi B}\left\{\frac{k\sqrt{k - 1}}{(1 - \lambda)^2(k + 1)\sqrt{k + 1}}\left[\cos^{-1}(2\lambda - 1) - \cos^{-1}\frac{1}{k}\right] - \right.$$

$$\frac{\lambda\sqrt{\lambda(k - 1)}}{(1 - \lambda)\sqrt{(1 - \lambda)(k + 1)}} + \frac{k - 1}{k(1 - \lambda)^2(k + 1)} +$$

$$\left.\frac{\left[2k - \lambda(k + 1)\right]^2}{2\sqrt{2}(1 - \lambda)^2(k + 1)\sqrt{k(k + 1)}}\cos^{-1}\frac{2k + \lambda(1 - 3k)}{2k - \lambda(k + 1)}\right\} \tag{A1}$$

For untapered wings; $\lambda = 1$; $km' = 1$:

$$C_{L_\alpha} = \frac{2}{\pi A'B}\left[\frac{(1 + A')^2}{2}\cos^{-1}\frac{A' - 1}{A' + 1} + \sqrt{A'} - \frac{8}{3} + \frac{5}{3}A'\sqrt{A'}\right] \tag{A2}$$

When the Mach line is behind the leading edge, that is, $B \cot \Lambda > 1$, and if $A' < \frac{4\lambda m'}{(1 + \lambda)(m' - 1)}$, there result:

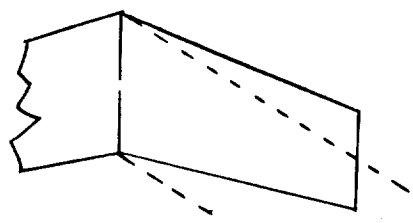

For tapered wings:

$$C_{L_\alpha} = \frac{1}{\pi B\sqrt{m'^2 - 1}}\left\{\frac{\left[4m'k + A'(k - 1)\right]^2}{2A'\left(k^2 - 1\right)}\left[\frac{1}{k}\cos^{-1}\frac{1}{m'} + \right.\right.$$

$$\left.\frac{k\sqrt{m'^2 - 1}}{\sqrt{(km' + 1)(km' - 1)}}\left(\cos^{-1}\frac{-1}{km'} - \cos^{-1}\frac{4km'(A' - 1) - A'(k + 3)}{4km' + A'(k - 1)}\right)\right] -$$

$$\frac{\left[4m'k - A'(k - 1)\right]^2}{4A'(k - 1)}\sqrt{\frac{m' + 1}{k(km' + 1)}}\cos^{-1}\frac{4km'(1 - A') + A'(3k + 1)}{4km' - A'(k - 1)} +$$

$$\left.\frac{\left[4m'k + A'(1 + 3k)\right]^2}{4A'(k + 1)}\sqrt{\frac{m' - 1}{k(km' + 1)}}\cos^{-1}\frac{4km'(A' - 1) + A'(k - 1)}{4km' + A'(3k + 1)}\right\} \tag{A3}$$

For unswept leading edges or for unswept trailing edges; $k = \infty$ or 0:

$$C_{L_\alpha} = \frac{4A'}{\pi B(1 - \lambda)}\left\{\frac{2}{J}\left[\cos^{-1}\left(1 - \frac{J}{2}\right) - \frac{\pi}{2}\right] - \frac{\lambda^2}{\sqrt{J\left[J - 4(1 - \lambda)\right]}}\cos^{-1}\frac{4 - 2\lambda - J}{2\lambda} + \frac{(2 - \lambda)^2}{\sqrt{J\left[J + 4(1 - \lambda)\right]}}\cos^{-1}\frac{J - 2\lambda}{2(2 - \lambda)}\right\} \tag{A4}$$

For untapered wings:

$$C_{L_\alpha} = \frac{4}{\pi A'B\sqrt{m'^2 - 1}}\left\{-\frac{m'^2\left(m'^2 - 2\right)}{(m'^2 - 1)}\cos^{-1}\frac{1}{m'} - \frac{m'^2}{\sqrt{m'^2 - 1}} + \left[\frac{m'^2(m' - 2)}{2(m' - 1)} + A'm'\right]\cos^{-1}\frac{m' - A'(m' - 1)}{m'} + \frac{(m' + A')^2\sqrt{m' - 1}}{2\sqrt{m' + 1}}\cos^{-1}\frac{m'(A' - 1)}{A' + m'} + \frac{m'\sqrt{A'\left[2m' - A'(m' - 1)\right]}}{2\sqrt{m' - 1}}\right\} \tag{A5}$$

If $A' > \frac{4\lambda m'}{(1 + \lambda)(m' - 1)}$:

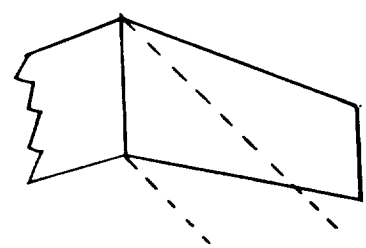

For tapered wings:

$$C_{L_\alpha} = \frac{1}{B\pi\sqrt{m'^2 - 1}}\left\{\frac{\left[4m'k + A'(k - 1)\right]^2}{2A'(k^2 - 1)}\left[\frac{1}{k}\cos^{-1}\frac{1}{m'} + \frac{k\sqrt{m'^2 - 1}}{\sqrt{(km' - 1)(km' + 1)}}\cos^{-1}\frac{-1}{km'}\right] - \frac{\pi\left[4km' - A'(k - 1)\right]^2}{4A'(k - 1)}\sqrt{\frac{m' + 1}{k(km' + 1)}}\right\} \tag{A6}$$

For unswept leading edges or for unswept trailing edges; $k = \infty$ or 0:

$$C_{L_\alpha} = \frac{4A'}{B(1 - \lambda)}\left\{\frac{1}{J} - \frac{\lambda^2}{\sqrt{J\left[J - 4(1 - \lambda)\right]}}\right\} \tag{A7}$$

For untapered wings; $\lambda = k = 1$:

$$C_{L_\alpha} = \frac{4}{\pi BA'\sqrt{m'^2 - 1}}\left\{-\frac{m'^2\left(m'^2 - 2\right)}{\left(m'^2 - 1\right)}\cos^{-1}\frac{1}{m'} - \frac{m'^2}{\sqrt{m'^2 - 1}} + \left[\frac{m'^2(m' - 2)}{2(m' - 1)} + A'm'\right]\pi\right\} \tag{A8}$$

Formulas for C_{l_p}

If the Mach line is coincident with the leading edge, that is, $B \cot \Lambda = 1$, there result:

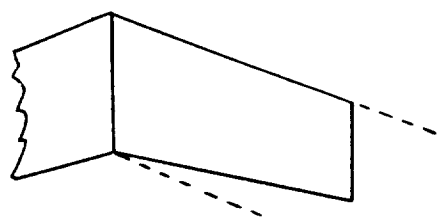

For tapered wings:

$$C_{l_p} = \left(\left\{\frac{\left[3J^3k^3(1 - k)^3 + 2J^2k^3(1 - k)^2(9k - 8)\right]}{(1 - k)^3} + \frac{\left[2Jk^3(1 - k)(15k^2 - 32k + 12) + 12k^4(k^2 + 4)\right]}{(1 - k)^3} + \frac{4\left[J^3(1 - k)(23k^2 + 10k + 2) + 4kJ^2(41k^2 - 5k - 1)\right]}{35} + \frac{4\left[-12k^2J(29k - 1) + 240k^3\right]}{35}\right\}\sqrt{\frac{J(1 - k) + 4k}{J(1 + k)}} + \frac{}{3J^2(1 + k)^3} +$$

(continued on next page)

$$\frac{8k^5(k^2 + 4)}{J^3(1 - k^2)^3\sqrt{k^2 - 1}}\left[\cos^{-1}\frac{1}{k} - \cos^{-1}\frac{J(1 - k) + 2k}{2k}\right] -$$

$$\left.\frac{8k^3(13k^2 + 2)}{3(1 - k^2)^3}\right)\left[\frac{-16}{3\pi B(1 + \lambda)}\right] + \frac{512}{3\pi B\sqrt{2}\,J(1 + \lambda)}\left(\frac{k}{k + 1}\right)^{3/2} \times$$

$$\left\{\left[2\lambda(41k^3 + 63k^2 + 11k - 11) - Jk(13k^2 + 29k - 4)\right]\frac{\left(\frac{J\lambda}{2}\right)^{3/2}}{48k(k + 1)^2} -\right.$$

$$\left[\frac{J^2(3k^2 + 3k + 20) + 4J\lambda(k^2 - 21k - 2) + 4\lambda^2k(23k + 3)}{64(k + 1)^2}\right] \times$$

$$\left[-\frac{1}{4}\left(\frac{J}{2} - \lambda\right)\sqrt{\frac{J\lambda}{2}} + \frac{1}{8}\left(\frac{J}{2} + \lambda\right)^2 \cos^{-1}\frac{J - 2\lambda}{J + 2\lambda}\right] + \frac{\lambda^{3/2}J^{5/2}}{6\sqrt{2}} -$$

$$\left.\frac{2\sqrt{2}}{5}\left(\frac{k}{k + 1}\right)\lambda^{5/2}J^{3/2} + \frac{4\sqrt{2}}{7}\left(\frac{k}{k + 1}\right)^2\lambda^{7/2}\sqrt{J}\right\} \tag{A9}$$

For unswept leading edges or for unswept trailing edges; $k = \infty$ or 0:

$$C_{l_p} = \frac{-16}{3\pi B(1 + \lambda)}\left\{\left[\frac{(13J^3 + 656J^2 - 342J + 540)}{105J^2}\right]\sqrt{\frac{4 - J}{J}} -\right.$$

$$\left.\frac{4}{J^3}\cos^{-1}\left(\frac{-2 + 2J - J^2}{2}\right)\right\} + \frac{512}{3\pi\sqrt{2}BJ^3(1 + \lambda)}\left\{\frac{(82\lambda - 13J)}{48}\left(\frac{J\lambda}{2}\right)^{3/2} -\right.$$

$$\left[\frac{3J^2 + 4J\lambda + 92\lambda^2}{64}\right]\left[-\frac{1}{4}\left(\frac{J}{2} - \lambda\right)\sqrt{\frac{J\lambda}{2}} + \frac{1}{8}\left(\frac{J}{2} + \lambda\right)^2 \cos^{-1}\frac{J - 2\lambda}{J + 2\lambda}\right] +$$

$$\left.\frac{\sqrt{2}\lambda^{3/2}J^{5/2}}{12} - \frac{2\sqrt{2}\lambda^{5/2}J^{3/2}}{5} + \frac{4\sqrt{2}\lambda^{7/2}\sqrt{J}}{7}\right\} \tag{A10}$$

For untapered wings; $\lambda = k = 1$:

$$C_{l_p} = \frac{16}{\pi BA'^3}\left[-\frac{8}{315} + \frac{(A' + 1)^2(13A'^2 - 22A' + 13)}{768}\cos^{-1}\frac{A' - 1}{A' + 1} + \sqrt{A'}\left(\frac{37A'^3}{2688} - \frac{41A'^2}{1920} + \frac{123A'}{5760} - \frac{37}{2688}\right)\right] \tag{A11}$$

When the Mach line is behind the leading edge, that is, $B \cot \Lambda > 1$, and if $A' < \frac{4\lambda m'}{(1 + \lambda)(m' - 1)}$, there result:

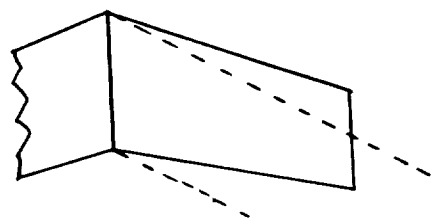

For tapered wings:

$$C_{l_p} = \frac{1}{B}\left\{\frac{-128m'^4k^3\left[4k^2 - m'^2(3k^2 + 1)\right]}{3\pi J^3(1 + \lambda)(m'^2 - 1)^{3/2}(1 - k^2)^3}\cos^{-1}\frac{1}{m'} + \right.$$

$$\frac{128m'^4k^3(1 + k^2 - 2m'^2k^2)}{3\pi J^3(1 + \lambda)(1 - k^2)^2(m'^2 - 1)(m'^2k^2 - 1)} -$$

$$\frac{128m'^4k^5\left[-4 + m'^2k^2(k^2 + 3)\right]}{3\pi J^3(1 + \lambda)(1 - k^2)^3(m'^2k^2 - 1)^{3/2}}\left[\cos^{-1}\frac{1}{km'} - \right.$$

$$\left.\cos^{-1}\frac{2m'k - J(m'k - 1)}{2m'k}\right] - \left\{J^4(1 - k)^4\left[24k^4m'^5 + 12k^3m'^4(k + 5) + \right.\right.$$

$$m'^3k^2(-17k^2 + 22k + 43) + m'^2k(-5k^3 - 48k^2 + 3k + 2) -$$

$$\left.m'(10k^3 + 45k^2 + 12k + 5) - (5k^2 + 14k + 5)\right] +$$

$$16km'J^3(1 - k)^3\left[8m'^5k^4 + 8k^3m'^4(k + 2) + m'^3k^2(-3k^2 + 14k + 5) + \right.$$

$$m'^2k(-3k^3 - 8k^2 + k - 6) - m'(6k^3 + 7k^2 + 8k + 3) -$$

$$\left.(3k^2 + 2k + 3)\right] + 32m'^2k^2J^2(1 - k)^3\left[-12k^3m'^4 - 9k^2m'^3(3 + k) + \right.$$

(continued on next page)

$$3m'^2k(k^2 - 7k - 6) + 3m'(2k^2 - 5k - 1) - 3(1 - k)\Big] +$$

$$256m'^3k^3J(1 - k)^2\Big[k^2m'^3(1 - k) + m'^2k(2 - k - k^2) +$$

$$m'(-2k^2 + k + 1) + (1 - k)\Big] + 256k^4m'^4\Big[8k^4m'^5 + 4m'^4k^3(7 - k) +$$

$$k^2m'^3(-9k^2 - 10k + 35) + km'^2(3k^3 - 32k^2 - 5k + 18) +$$

$$m'(6k^3 - 37k^2 + 4k + 3) + (3k^2 - 14k +$$

$$3)\Big]\Bigg\} \frac{\cos^{-1}\dfrac{J(1 + k - 2km') + 4km'}{J(1 - k) + 4km'}}{96\pi J^3(1 + \lambda)k(1 - k)^3(m'^2 - 1)(m'k + 1)^3\sqrt{k(m'k + 1)(m' - 1)}} -$$

$$\Big\{J^4(1 + k)^4\Big[24k^4m'^5 + 12k^3m'^4(5 - k) + m'^3k^2(-17k^2 - 22k + 43) +$$

$$km'^2(5k^3 - 48k^2 - 3k + 2) + m'(10k^3 - 45k^2 + 12k - 5) +$$

$$(5k^2 - 14k + 5)\Big] + 16km'J^3(1 + k)^3\Big[8k^4m'^5 + 8k^3m'^4(2 - k) +$$

$$k^2m'^3(-3k^2 - 14k + 5) + km'^2(3k^3 - 8k^2 - k - 6) + m'(6k^3 - 7k^2 +$$

$$8k - 3) + (3k^2 - 2k + 3)\Big] + 32k^2m'^2J^2(1 + k)^3\Big[-12k^3m'^4 -$$

$$9k^2m'^3(3 - k) + 3km'^2(k^2 + 7k - 6) + 3m'(2k^2 + 5k - 1) +$$

$$3(1 + k)^2\Big] + 256k^3m'^3J(1 + k)^2\Big[k^2m'^3(1 + k) + km'^2(2 + k - k^2) +$$

$$m'(-2k^3 - 3k^2 + 1) - (1 + k)\Big] + 256k^4m'^4\Big[8k^4m'^5 + 4k^3m'^4(k + 7) +$$

$$k^2m'^3(-9k^2 + 10k + 35) + km'^2(-3k^3 - 32k^2 + 5k + 18) +$$

$$m'(-6k^3 - 37k^2 - 4k + 3) - (3k^2 + 14k +$$

$$3)\Big]\Bigg\} \frac{\cos^{-1}\dfrac{J(k - 1 + 2km') - 4km'}{J(1 + k) + 4km'}}{96\pi J^3(1 + \lambda)k(1 + k)^3(m'^2 - 1)(m'k + 1)^3\sqrt{k(m'k + 1)(m' + 1)}} -$$

$$\Big\{J^3(1 - k^2)^2\Big[-2k^7m'^7 + 4k^6m'^6 - k^5m'^5(5k^2 - 7) + k^4m'^4(5k^2 - 13) +$$

$$2k^3m'^3(5k^2 - 4) - 2k^2m'^2(5k^2 - 7) - km'(5k^2 - 3) + 5(k^2 - 1)\Big] +$$

(continued on next page)

$$4J^2(1 - k^2)^2km'(13k^6m'^6 - 6k^5m'^5 - 33k^4m'^4 + 12k^3m'^3 + 27k^2m'^2 -$$

$$6km' - 7) + 16J(1 - k^2)k^2m'^2\Big[2k^7m'^7 + 2k^6m'^6 + 3k^5m'^5(k^2 - 3) -$$

$$3k^4m'^4(k^2 + 1) + 6k^3m'^3(2 - k^2) + 6k^4m'^2 + km'(3k^2 - 5) -$$

$$(3k^2 - 1)\Big] + 64k^3m'^3\Big[-8k^7m'^7 - k^6m'^6(k^2 + 7) + 4k^5m'^5(k^2 + 5) +$$

$$k^4m'^4(7k^2 + 17) - 8k^3m'^3(k^2 + 2) - k^2m'^2(11k^2 + 13) + 4km'(k^2 + 1) +$$

$$(5k^2 + 3)\Big]\Bigg\} \frac{\sqrt{\dfrac{J\left[4m'k - J(km' - 1)\right]}{km' + 1}}}{24\pi J^3(1 + \lambda)k(m'^2 - 1)(1 - k^2)^2(k^2m'^2 - 1)^3}\Bigg\} \qquad \text{(A12)}$$

For untapered wings; $\lambda = k = 1$:

$$C_{l_p} = \frac{-16}{\pi BA'^3}\Bigg\{\Big[A'^4(6m'^2 + 6m' + 1) + 4A'^3m'(2m'^2 - 1) - 6A'^2m'^2(2m' + 1) +$$

$$4A'm'^3 + m'^4(2m'^2 + 6m' + 5)\Big] \frac{\cos^{-1}\dfrac{m'(A' - 1)}{A' + m'}}{192(m' + 1)^3} + \Big[m'^4(2m'^4 -$$

$$4m'^3 - 2m'^2 + 9m') + 8A'^3m'(m' - 1)^2(m'^2 - 1) - 12A'^2m'^3(m' - 1)^2 +$$

$$4A'm'^3(m' - 1)^2\Big] \frac{\cos^{-1}\dfrac{m' - A'(m' - 1)}{m'}}{192(m' - 1)^2(m'^2 - 1)\sqrt{m'^2 - 1}} +$$

$$\frac{m'^4(-8m'^2 + 4m'^4 - m'^6)}{48(m'^2 - 1)^3\sqrt{m'^2 - 1}} \cos^{-1}\frac{1}{m'} + \frac{m'^4(8 + 10m'^2 - 3m'^4)}{144(m'^2 - 1)^3} +$$

$$\Big[3A'^3(-m'^4 + 3m'^3 - 3m'^2 + m') + A'^2m'(2m'^4 + 39m'^3 - 61m'^2 -$$

$$3m' + 23) + A'm'^2(-14 + 34m' - 19m'^2 + 2m'^3 - 3m'^4) + 3m'^3(-5 -$$

$$6m'^2 - m'^3 + 2m'^4)\Big] \frac{\sqrt{\dfrac{A'm'}{2} - \dfrac{A'^2(m' - 1)}{4}}}{288(m'^2 - 1)^2(m' - 1)\sqrt{m' + 1}}\Bigg\} \qquad \text{(A13)}$$

If $A' > \frac{4\lambda m'}{(1 + \lambda)(m' - 1)}$:

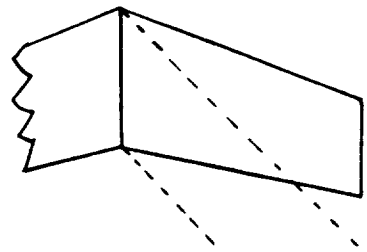

For tapered wings:

$$
\begin{aligned}
C_{l_p} = \frac{1}{B}\Bigg\{ & \frac{-128m'^4k^3\left[4k^2 - m'^2(3k^2 + 1)\right]}{3\pi J^3(1 + \lambda)(m'^2 - 1)^{3/2}(1 - k^2)^3} \cos^{-1}\frac{1}{m'} + \\
& \frac{128k^3m'^4(1 + k^2 - 2m'^2k^2)}{3\pi J^3(1 + \lambda)(1 - k^2)^2(m'^2 - 1)(k^2m'^2 - 1)} + \\
& \frac{128k^5m'^4\left[-4 + m'^2k^2(k^2 + 3)\right]}{3\pi J^3(1 + \lambda)(1 - k^2)^3(m'^2k^2 - 1)^{3/2}} \cos^{-1}\frac{-1}{km'} - \\
& \Big\{J^4(1 - k)^4\Big[24k^4m'^5 + 12k^3m'^4(k + 5) + k^2m'^3(-17k^2 + 22k + 43) + \\
& km'^2(-5k^3 - 48k^2 + 3k + 2) - m'(10k^3 + 45k^2 + 12k + 5) - \\
& (5k^2 + 14k + 5)\Big] + 16km'J^3(1 - k)^3\Big[8k^4m'^5 + 8k^3m'^4(k + 2) + \\
& k^2m'^3(-3k^2 + 14k + 5) + km'^2(-3k^3 - 8k^2 + k - 6) - m'(6k^3 + 7k^2 + \\
& 8k + 3) - (3k^2 + 2k + 3)\Big] + 32k^2m'^2J^2(1 - k)^3\Big[-12k^3m'^4 - \\
& 9k^2m'^3(3 + k) + 3km'^2(k^2 - 7k - 6) + 3m'(2k^2 - 5k - 1) - \\
& 3(1 - k)\Big] + 256k^3m'^3J(1 - k)^2\Big[k^2m'^3(1 - k) + km'^2(2 - k - k^2) + \\
& m'(-2k^2 + k + 1) + (1 - k)\Big] + 256k^4m'^4\Big[8k^4m'^5 + 4k^3m'^4(7 - k) + \\
& k^2m'^3(-9k^2 - 10k + 35) + km'^2(3k^3 - 32k^2 - 5k + 18) + m'(6k^3 - \\
& 37k^2 + 4k + 3) + (3k^2 - 14k + \\
& 3)\Big]\Big\} \frac{1}{96J^3(1 + \lambda)k(1 - k)^3(m'^2 - 1)(km' + 1)^3\sqrt{k(km' + 1)(m' - 1)}}\Bigg\}
\end{aligned}
\tag{A14}
$$

For unswept leading edges or for unswept trailing edges; $k = \infty$ or 0:

$$C_{l_p} = \frac{-1}{B(1 - \lambda)^3(1 + \lambda)}\left\{\frac{1}{3} + \lambda^2\left[2\lambda(1 - \lambda)^2(5\lambda - 3) + 6J(1 - \lambda)(\lambda^2 - 4\lambda + 4) + J^2(-3\lambda^2 + 8\lambda - 6)\right]\frac{1}{3\left[J - 4(1 - \lambda)\right]\sqrt{J\left[J - 4(1 - \lambda)\right]}}\right\} \tag{A15}$$

For $\lambda = 0$:

$$C_{l_p} = \frac{128k^3m'^4}{3\pi BA'^3(1 - k^2)^2}\left\{\frac{1 + k^2 - 2k^2m'^2}{(m'^2 - 1)(k^2m'^2 - 1)} + \frac{m'^2(3k^2 + 1) - 4k^2}{(1 - k^2)(m'^2 - 1)^{3/2}}\cos^{-1}\frac{1}{m'} + \frac{k^4m'^2(k^2 + 3) - 4k^2}{(1 - k^2)(k^2m'^2 - 1)^{3/2}}\cos^{-1}\frac{-1}{km'}\right\} \tag{A16}$$

For untapered wings; $\lambda = k = 1$:

$$C_{l_p} = \frac{-16}{\pi A'^3B}\left\{\left[m'^4(2m'^4 - 4m'^3 - 2m'^2 + 9m') + 8A'^3m'(m' - 1)^2(m'^2 - 1) - 12A'^2m'^3(m' - 1)^2 + 4A'm'^3(m' - 1)^2\right]\frac{\pi}{192(m' - 1)^2(m'^2 - 1)\sqrt{m'^2 - 1}} + \frac{m'^4(-3m'^4 + 10m'^2 + 8)}{144(m'^2 - 1)^3} + \frac{m'^4(-m'^6 + 4m'^4 - 8m'^2)}{48(m'^2 - 1)^3\sqrt{m'^2 - 1}}\cos^{-1}\frac{1}{m'}\right\} \tag{A17}$$

REFERENCES

1. Lagerstrom, P. A., Wall, D., and Graham, M. E.: Formulas in Three-Dimensional Wing Theory. Rep. No. SM-11901, Douglas Aircraft Co., Inc., July 8, 1946.

2. Lagerstrom, P. A., and Graham, Martha E.: Some Aerodynamic Formulas in Linearized Supersonic Theory for Damping in Roll and Effect of Twist for Trapezoidal Wings. Rep. No. SM-13200, Douglas Aircraft Co., Inc., March 12, 1948.

3. Jones, Arthur L., and Alksne, Alberta: The Damping Due to Roll of Triangular, Trapezoidal, and Related Plan Forms in Supersonic Flow. NACA TN 1548, 1948.

4. Cohen, Doris: The Theoretical Lift of Flat Swept-Back Wings at Supersonic Speeds. NACA TN 1555, 1948.

5. Harmon, Sidney M.: Stability Derivatives at Supersonic Speeds of Thin Rectangular Wings with Diagonals ahead of Tip Mach Lines. NACA Rep. 925, 1949.

6. Malvestuto, Frank S., Jr., and Margolis, Kenneth: Theoretical Stability Derivatives of Thin Sweptback Wings Tapered to a Point with Sweptback or Sweptforward Trailing Edges for a Limited Range of Supersonic Speeds. NACA TN 1761, 1949.

7. Malvestuto, Frank S., Jr., Margolis, Kenneth, and Ribner, Herbert S.: Theoretical Lift and Damping in Roll of Thin Sweptback Wings of Arbitrary Taper and Sweep at Supersonic Speeds. Subsonic Leading Edges and Supersonic Trailing Edges. NACA TN 1860, 1949.

8. Harmon, Sidney M.: Theoretical Relations between the Stability Derivatives of a Wing in Direct and in Reverse Supersonic Flow. NACA TN 1943, 1949.

9. Brown, Clinton E.: The Reversibility Theorem for Thin Airfoils in Subsonic and Supersonic Flow. NACA TN 1944, 1949.

10. Hayes, Wallace D.: Reversed Flow Theorems in Supersonic Aerodynamics. Rep. No. AL-755, North American Aviation, Inc., Aug. 20, 1948.

11. Glauert, H.: A Non-Dimensional Form of the Stability Equations of an Aeroplane. R.&M. No. 1093, British A.R.C., 1927.

12. Brown, Clinton E.: Theoretical Lift and Drag of Thin Triangular Wings at Supersonic Speeds. NACA Rep. 839, 1946.

13. Brown, Clinton E., and Adams, Mac C.: Damping in Pitch and Roll of Triangular Wings at Supersonic Speeds. NACA Rep. 892, 1948.

14. Evvard, John C.: Distribution of Wave Drag and Lift in the Vicinity of Wing Tips at Supersonic Speeds. NACA TN 1382, 1947.

15. Evvard, John C.: Theoretical Distribution of Lift on Thin Wings at Supersonic Speeds (An Extension). NACA TN 1585, 1948.

16. Moeckel, W. E., and Evvard, J. C.: Load Distributions Due to Steady Roll and Pitch for Thin Wings at Supersonic Speeds. NACA TN 1689, 1948.

TABLE I.- GENERALIZED FORMULAS FOR ϕ DISTRIBUTIONS

$$\left[B \cot \Lambda \geqq 1;\ \left|B \cot \Lambda_{TE}\right| \geqq 1;\ BA \geqq \frac{4B \cot \Lambda}{(1 + \lambda)(1 + B \cot \Lambda)}\ \text{(See fig. 1.)}\right]$$

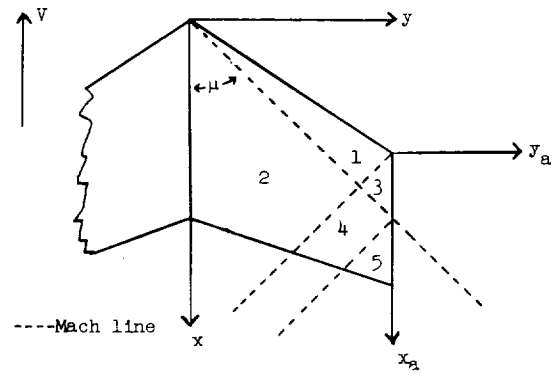

Region (see sketch)	Formula for ϕ contributed by α
1	$\dfrac{V\alpha(mx - y)}{\sqrt{B^2m^2 - 1}}$
2	$\dfrac{V\alpha}{\pi\sqrt{B^2m^2 - 1}}\left[(mx - y)\cos^{-1}\dfrac{x - B^2my}{B(mx - y)} + (mx + y)\cos^{-1}\dfrac{x + B^2my}{B(mx + y)}\right]$
3	$\dfrac{V\alpha}{\pi\sqrt{B^2m^2 - 1}}\left[(mx_a - y_a)\cos^{-1}\dfrac{mx_a + y_a(2Bm + 1)}{mx_a - y_a} + 2\sqrt{-my_a(x_a + By_a)(Bm + 1)}\right]$
4	$\dfrac{V\alpha}{\pi\sqrt{B^2m^2 - 1}}\left\{(mx_a - y_a)\left[\cos^{-1}\dfrac{mx_a + y_a(2Bm + 1)}{mx_a - y_a} - \cos^{-1}\dfrac{-mx_a + B^2m^2y_a + h(B^2m^2 - 1)}{Bm(mx_a - y_a)}\right] + (mx_a + 2h + y_a)\cos^{-1}\dfrac{mx_a + B^2m^2y_a + h(B^2m^2 + 1)}{Bm(mx_a + y_a + 2h)} + 2\sqrt{-my_a(x_a + By_a)(Bm + 1)}\right\}$
5	$\dfrac{V\alpha}{\pi\sqrt{B^2m^2 - 1}}\left[(mx_a + y_a + 2h)\cos^{-1}\dfrac{mx_a + y_a(2Bm - 1) + 2h}{mx_a + y_a + 2h} + 2\sqrt{-y_a(mx_a + Bmy_a + 2h)(Bm - 1)}\right]$

NACA

TABLE I.- GENERALIZED FORMULAS FOR ϕ DISTRIBUTIONS - Concluded

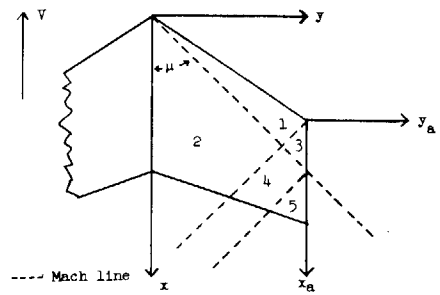

Region (see sketch)	Formula for ϕ contributed by p
1	$\frac{p}{2(B^2m^2 - 1)^{3/2}}\left\{(mx - y)\left[-mx + y(2B^2m^2 - 1)\right]\right\}$
2	$\frac{p}{\pi(B^2m^2 - 1)}\left(\frac{1}{\sqrt{B^2m^2 - 1}}\left\{\frac{(mx - y)\left[-mx + y(2B^2m^2 - 1)\right]}{2}\cos^{-1}\frac{x - B^2my}{B(mx - y)} + \frac{(mx + y)\left[mx - y(1 - 2B^2m^2)\right]}{2}\cos^{-1}\frac{x + B^2my}{B(mx + y)}\right\} - my\sqrt{x^2 - B^2y^2}\right)$
3	$\frac{p}{\pi(B^2m^2 - 1)^{3/2}}\left\{\frac{(mx_a - y_a)\left[-mx_a + y_a(2B^2m^2 - 1) + 2h(B^2m^2 - 1)\right]}{2}\cos^{-1}\frac{mx_a + y_a(2Bm + 1)}{mx_a - y_a} - \frac{mx_a(4Bm + 1) + 3y_a - 2Bmy_a(Bm + 1) - 6h(B^2m^2 - 1)}{3}\sqrt{-my_a(x_a + By_a)(Bm + 1)}\right\}$
4	$\frac{p}{\pi}\left(\frac{1}{(B^2m^2 - 1)^{3/2}}\left\{-\frac{(mx_a - y_a)\left[mx_a - y_a(2B^2m^2 - 1) - 2h(B^2m^2 - 1)\right]}{2}\left[\cos^{-1}\frac{mx_a + y_a(2Bm + 1)}{mx_a - y_a} - \cos^{-1}\frac{-mx_a + B^2m^2y_a + h(B^2m^2 - 1)}{Bm(mx_a - y_a)}\right] + \frac{(mx_a + 2h + y_a)\left[mx_a + y_a(2B^2m^2 - 1) + 2B^2m^2h\right]}{2}\cos^{-1}\frac{mx_a + B^2m^2y_a + h(B^2m^2 + 1)}{Bm(mx_a + y_a + 2h)} + \frac{-mx_a(4Bm + 1) + y_a(2B^2m^2 + 2Bm - 3) + 6h(B^2m^2 - 1)}{3}\sqrt{-my_a(x + By_a)(Bm + 1)}\right\} - \frac{y_a + h}{B^2m^2 - 1}\sqrt{m^2x_a^2 - B^2m^2y_a^2 + 2hm(x_a - B^2my_a) - h^2(B^2m^2 - 1)}\right)$
5	$\frac{p}{\pi(B^2m^2 - 1)^{3/2}}\left[\frac{m^2x_a^2 + 2B^2m^3x_ay_a + 2hmx_a(B^2m^2 + 1) + 2hy_a(3B^2m^2 - 1) + y_a^2(2B^2m^2 - 1) + 4B^2m^2h^2}{2}\cos^{-1}\frac{mx_a + y_a(2Bm - 1) + 2h}{mx_a + y_a + 2h} + \frac{-mx_a(4Bm - 1) + y_a(2B^2m^2 - 2Bm - 3) + 2h(3B^2m^2 - 4Bm - 2)}{3}\sqrt{-y_a(mx_a + Bmy_a + 2h)(Bm - 1)}\right]$

TABLE II.- GENERALIZED FORMULAS FOR ΔC_p DISTRIBUTIONS CAUSED BY CONSTANT ANGLE OF ATTACK AND BY STEADY ROLLING

$$\left[B \cot \Lambda \geqq 1;\ \left|B \cot \Lambda_{TE}\right| \geqq 1;\ BA \geqq \frac{4B \cot \Lambda}{(1 + \lambda)(1 + B \cot \Lambda)} \text{ (See fig. 1.)}\right]$$

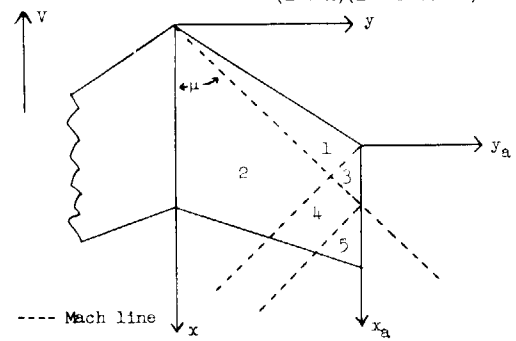

Region (see sketch)	Formula for ΔC_p contributed by α	Formula for ΔC_p contributed by p
1	$\frac{4\alpha m}{\sqrt{B^2m^2 - 1}}$	$\frac{4pm^2x(B^2m^2\nu - 1)}{V(B^2m^2 - 1)^{3/2}}$
2	$\frac{4\alpha m}{\pi\sqrt{B^2m^2 - 1}}\left[\cos^{-1}\frac{1 + B^2m^2\nu}{Bm(1 + \nu)} + \cos^{-1}\frac{1 - B^2m^2\nu}{Bm(1 - \nu)}\right]$	$\frac{4pm^2x}{\pi V(B^2m^2 - 1)^{3/2}}\left[(1 + B^2m^2\nu)\cos^{-1}\frac{1 + B^2m^2\nu}{Bm(1 + \nu)} - (1 - B^2m^2\nu)\cos^{-1}\frac{1 - B^2m^2\nu}{Bm(1 - \nu)}\right]$
3	$\frac{4\alpha m}{\sqrt{B^2m^2 - 1}} + \left(\Delta C_{p_t}\right)_\alpha{}^*$	$\frac{4pm^2x(B^2m^2\nu - 1)}{V(B^2m^2 - 1)^{3/2}} + \left(\Delta C_{p_t}\right)_p{}^*$
4	$\left(\Delta C_p\right)_{\text{Region 2}} + \left(\Delta C_{p_t}\right)_\alpha{}^*$	$\left(\Delta C_p\right)_{\text{Region 2}} + \left(\Delta C_{p_t}\right)_p{}^*$
5	$\frac{4\alpha m}{\pi\sqrt{B^2m^2 - 1}}\cos^{-1}\frac{mx_a - y_a(1 - 2Bm) + 2h}{mx_a + y_a + 2h}$	$\frac{4pm}{\pi V(B^2m^2 - 1)^{3/2}}\left\{\left[mx_a + B^2m^2y_a + h(B^2m^2 + 1)\right]\cos^{-1}\frac{mx_a - y_a(1 - 2Bm) + 2h}{mx_a + y_a + 2h} - 2Bm\sqrt{-y_a(Bm - 1)(mx_a + Bmy_a + 2h)}\right\}$

$$^*\left(\Delta C_{p_t}\right)_\alpha = -\frac{4\alpha m}{\pi\sqrt{B^2m^2 - 1}}\cos^{-1}\frac{-\left[mx_a + y_a(2Bm + 1)\right]}{mx_a - y_a}$$

$$\left(\Delta C_{p_t}\right)_p = \frac{4pm}{\pi V(B^2m^2 - 1)^{3/2}}\left\{\left[mx_a - B^2m^2y_a - h(B^2m^2 - 1)\right]\cos^{-1}\frac{-\left[mx_a + y_a(2Bm + 1)\right]}{mx_a - y_a} - 2Bm\sqrt{-my_a(x_a + By_a)(Bm + 1)}\right\}$$

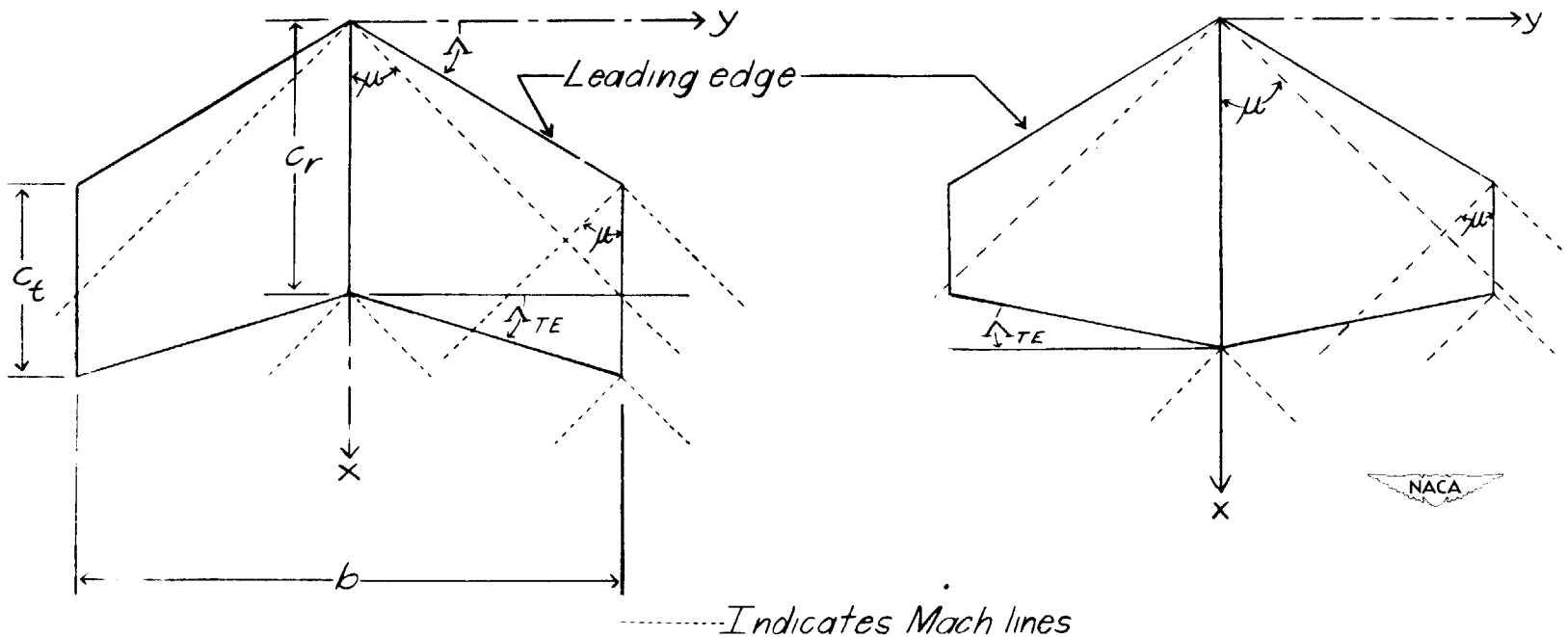

(a) Positive Λ and Λ_{TE}.

(b) Positive Λ and negative Λ_{TE}.

Figure 1.- Wing configurations to which all ϕ and ΔC_p distributions and C_{L_α} and C_{l_p} derivatives are applicable. Supersonic leading and trailing edges; streamwise tips. Note that Mach line from leading edge of center section may intersect either tip or trailing edge and also that Mach line from either tip does not intersect remote half-wing. $B \cot \Lambda \geqq 1$; $|B \cot \Lambda_{TE}| \geqq 1$; $BA > \frac{4B \cot \Lambda}{(1 + \lambda)(1 + B \cot \Lambda)}$.

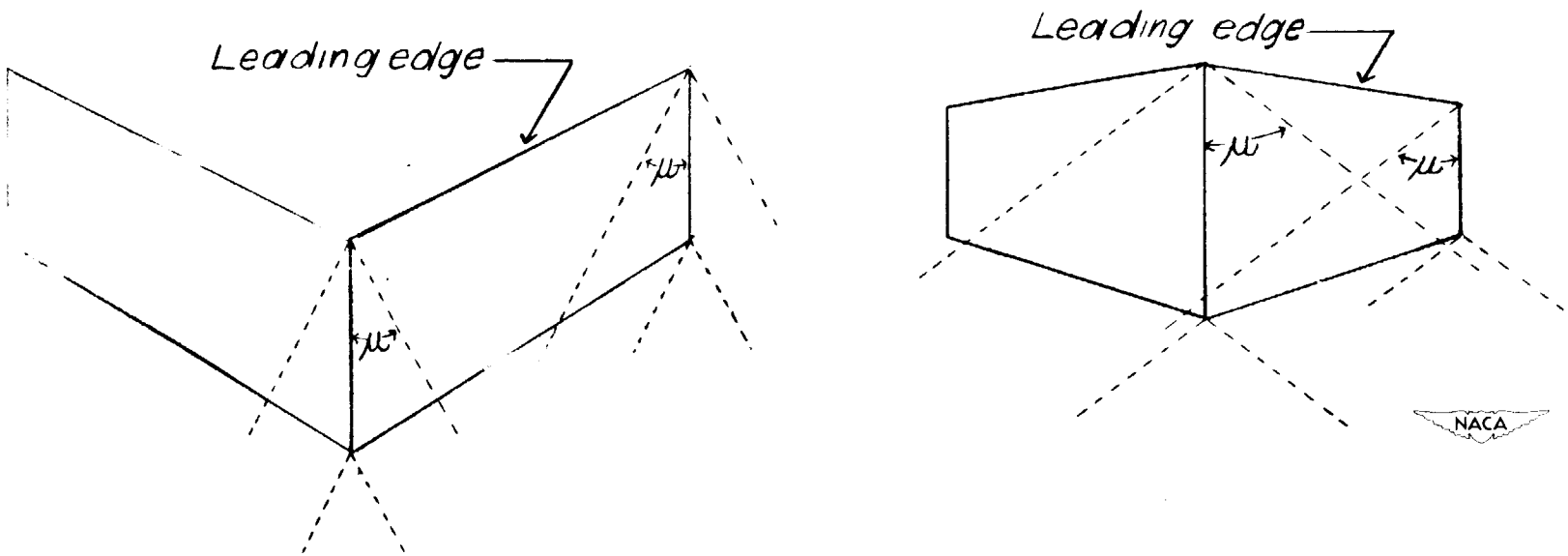

(a) Negative Λ and Λ_{TE}.

(b) Mach line from either tip intersects remote half-wing on condition that Mach line from leading edge of center section intersects wing trailing edge.

Figure 2.- Additional wing configurations to which values for C_{L_α} and C_{l_p} may be extended by use of theorem of reversibility.

$$|B \cot \Lambda| \geqq 1; \quad BA < \frac{4B \cot \Lambda}{(1 + \lambda)(1 + B \cot \Lambda)} \geqq \frac{4\lambda B \cot \Lambda}{(1 + \lambda)(B \cot \Lambda - 1)}.$$

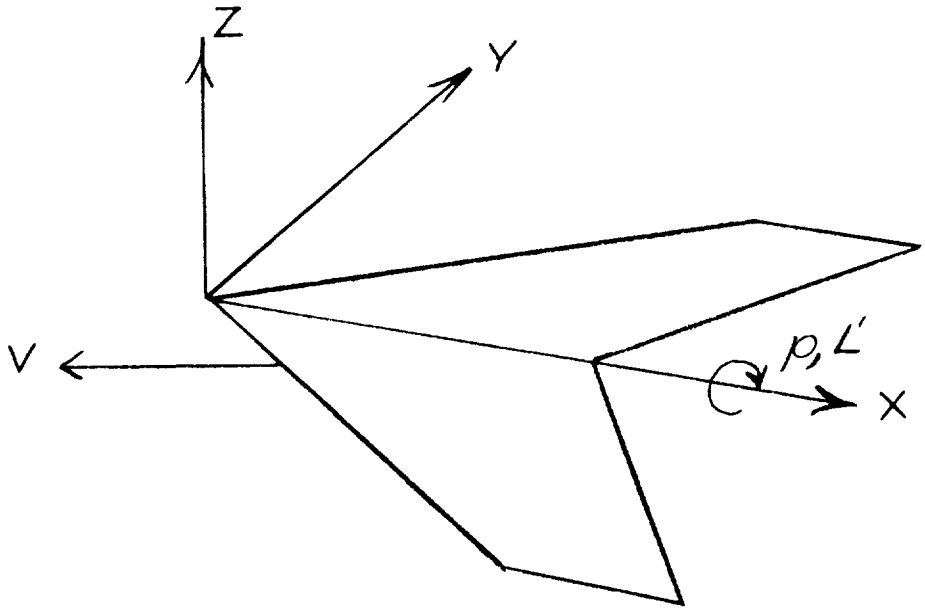

(a) Notation and body axes used in analysis.

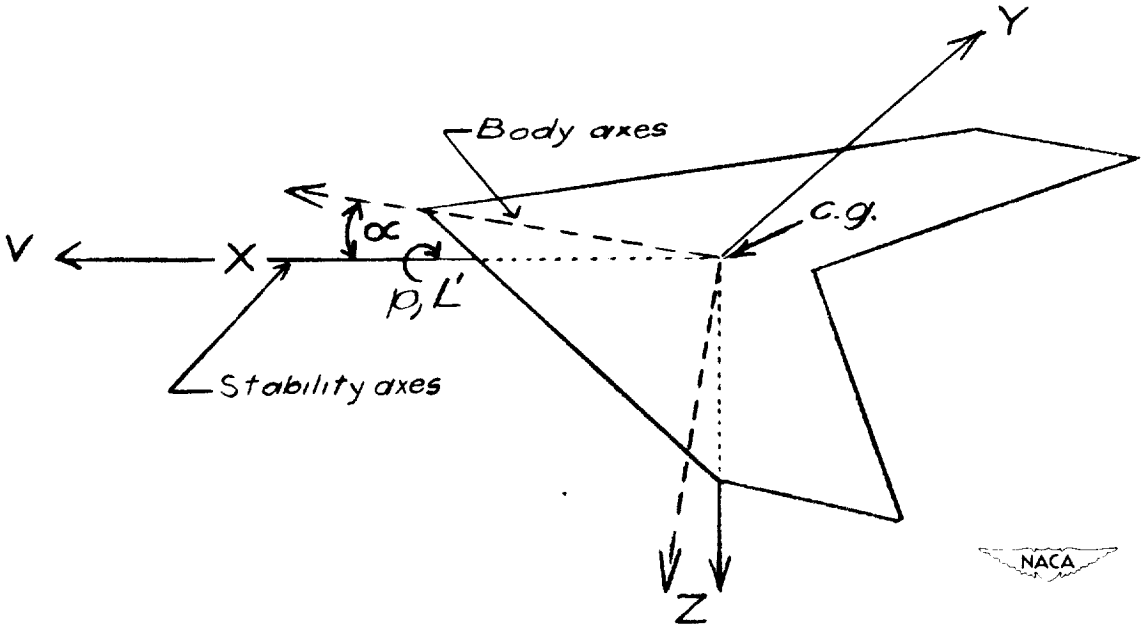

(b) Stability axes. (Corresponding body axes dashed for comparison.)

Figure 3.- System of axes and associated data.

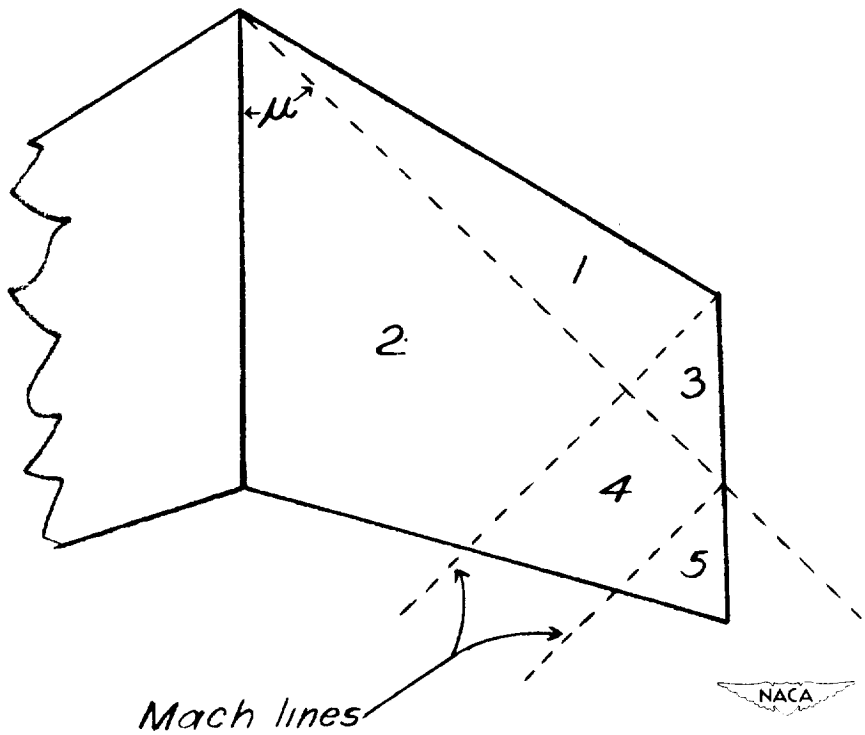

Figure 4.- Regions of similar disturbances for velocity potential and pressure distributions.

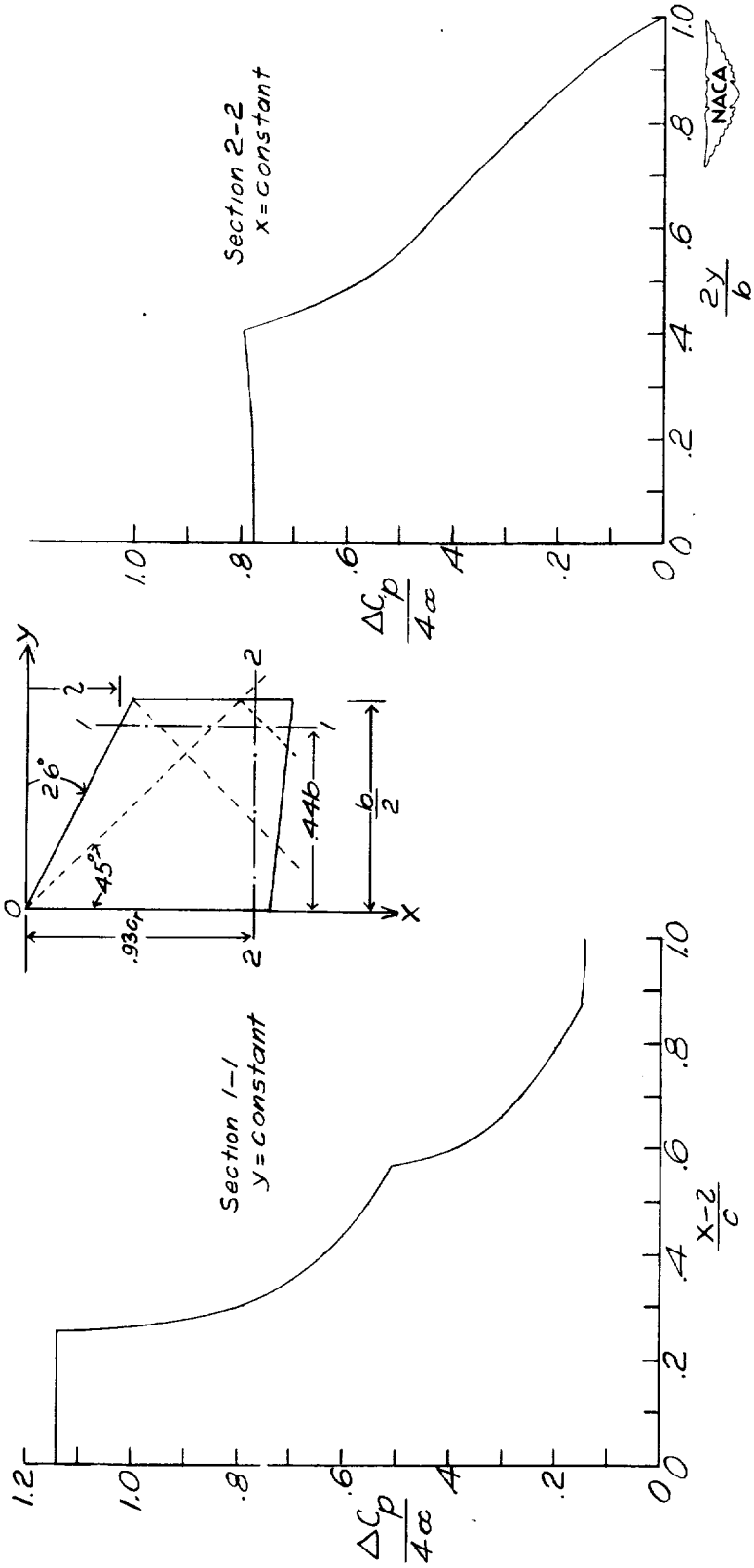

Figure 5.- Chordwise and spanwise pressure distributions for angle of attack in sectional planes.

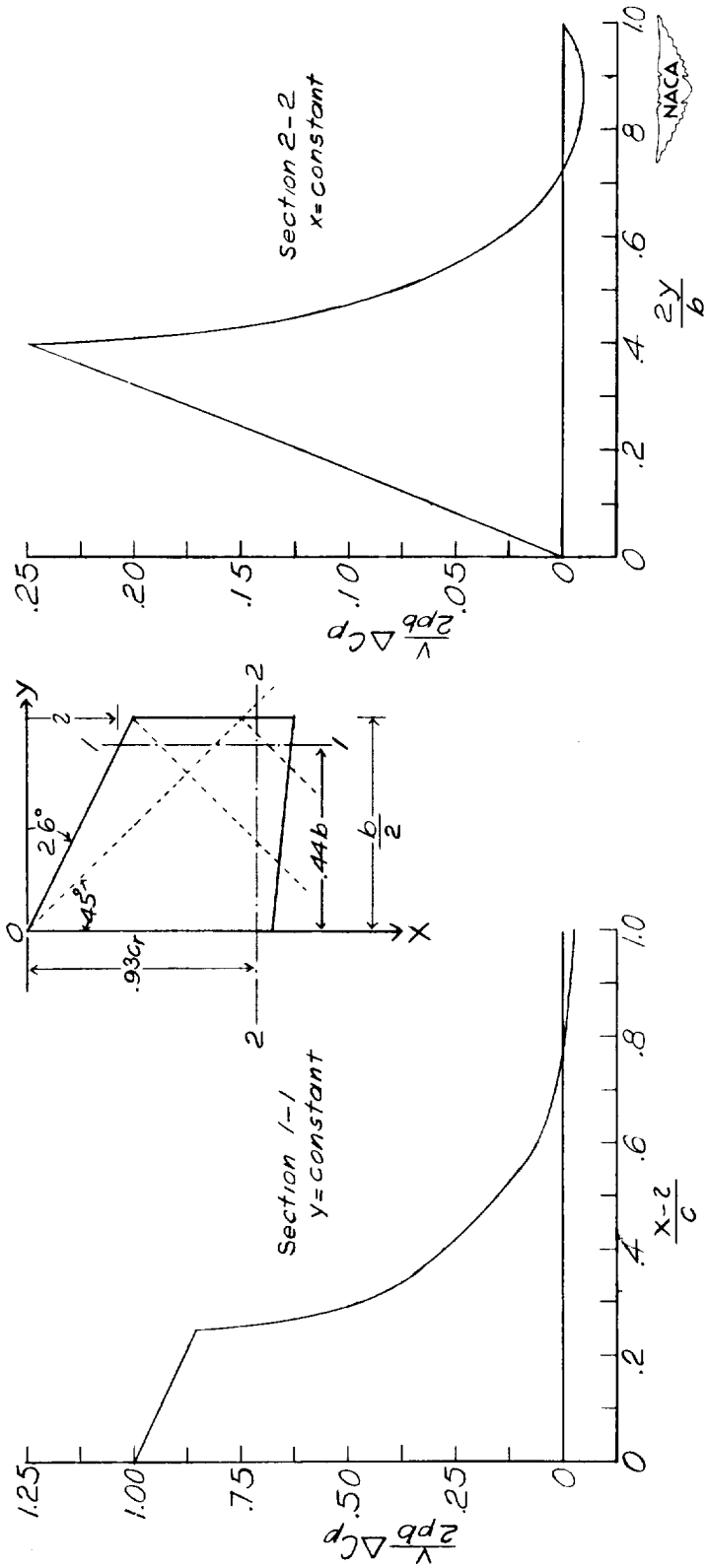

Figure 6.- Chordwise and spanwise pressure distributions for rolling in sectional planes.

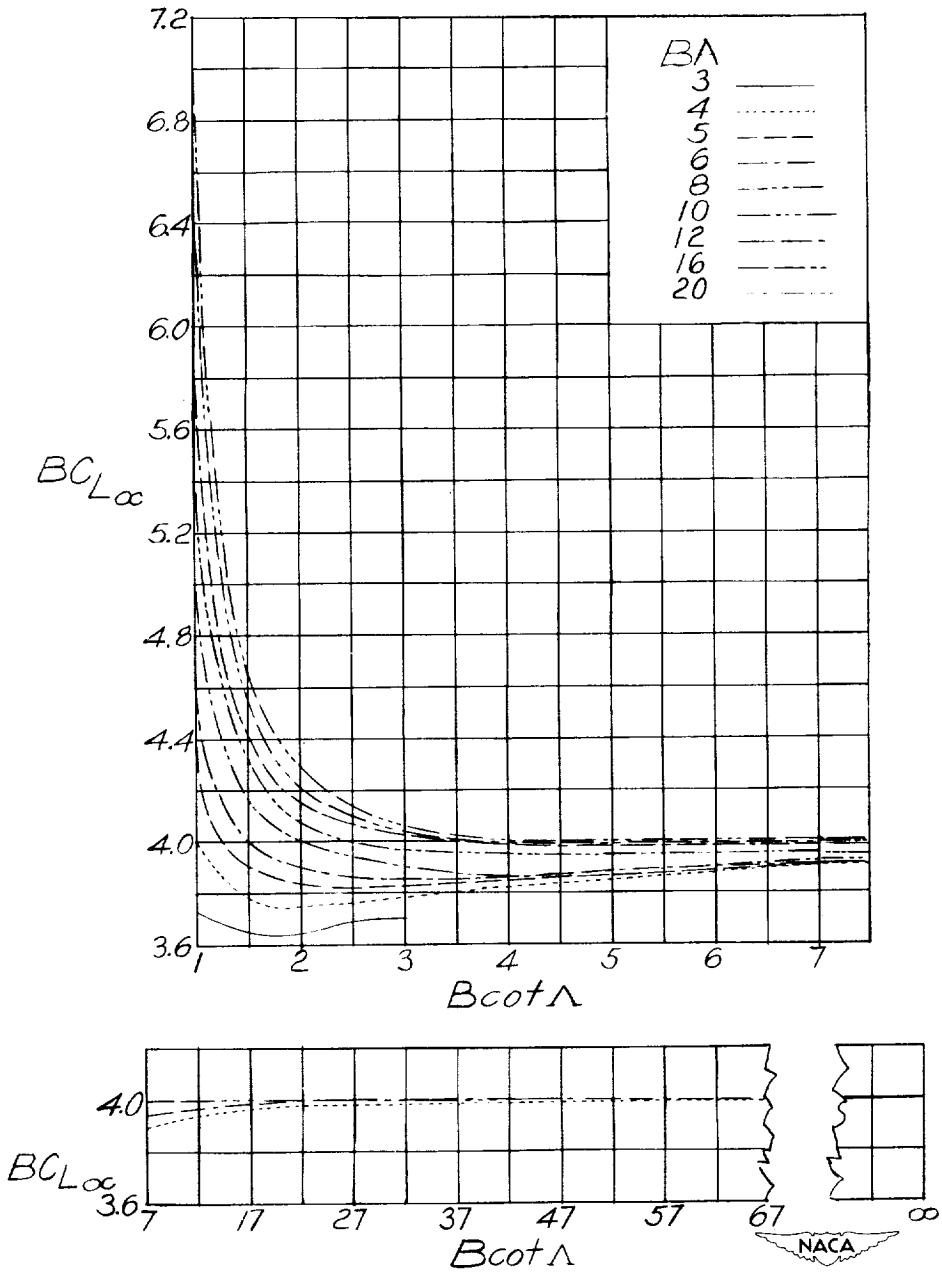

(a) Taper ratio $\lambda = 0$.

Figure 7.- Variation of BC_{L_α} with sweepback-angle parameter for various values of aspect-ratio parameter and taper ratio.

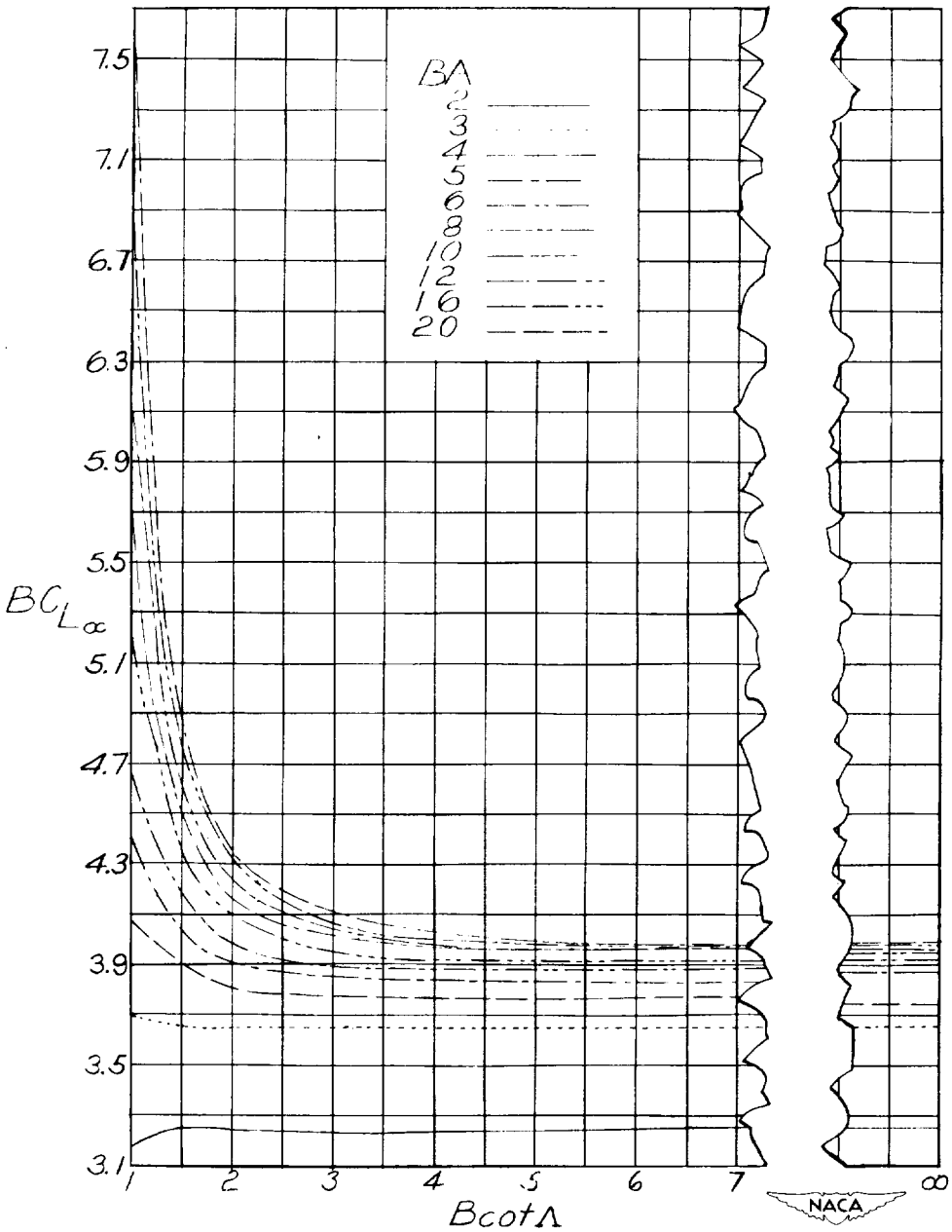

(b) Taper ratio $\lambda = 0.25$.

Figure 7.- Continued.

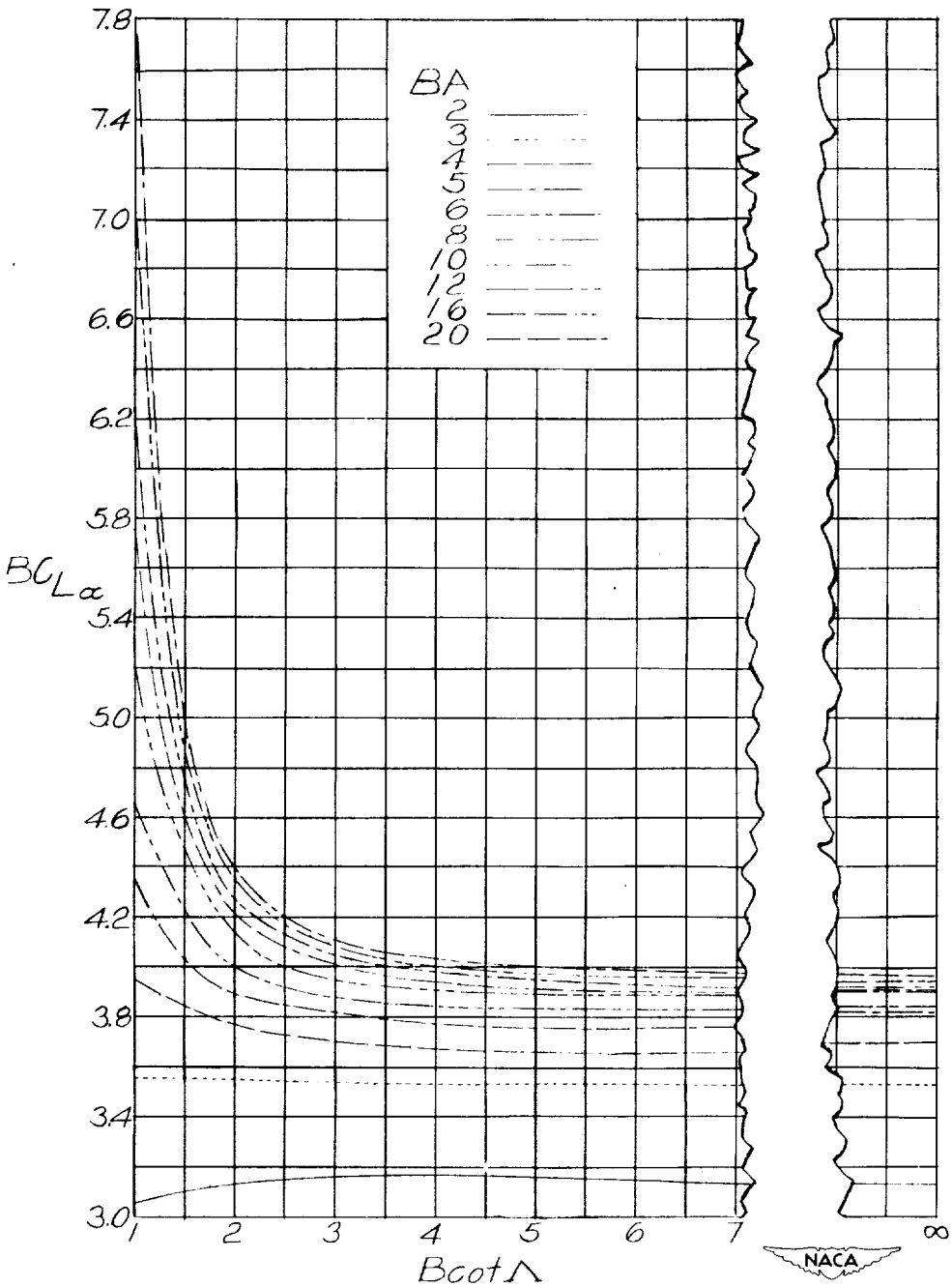

(c) Taper ratio $\lambda = 0.50$.

Figure 7.- Continued.

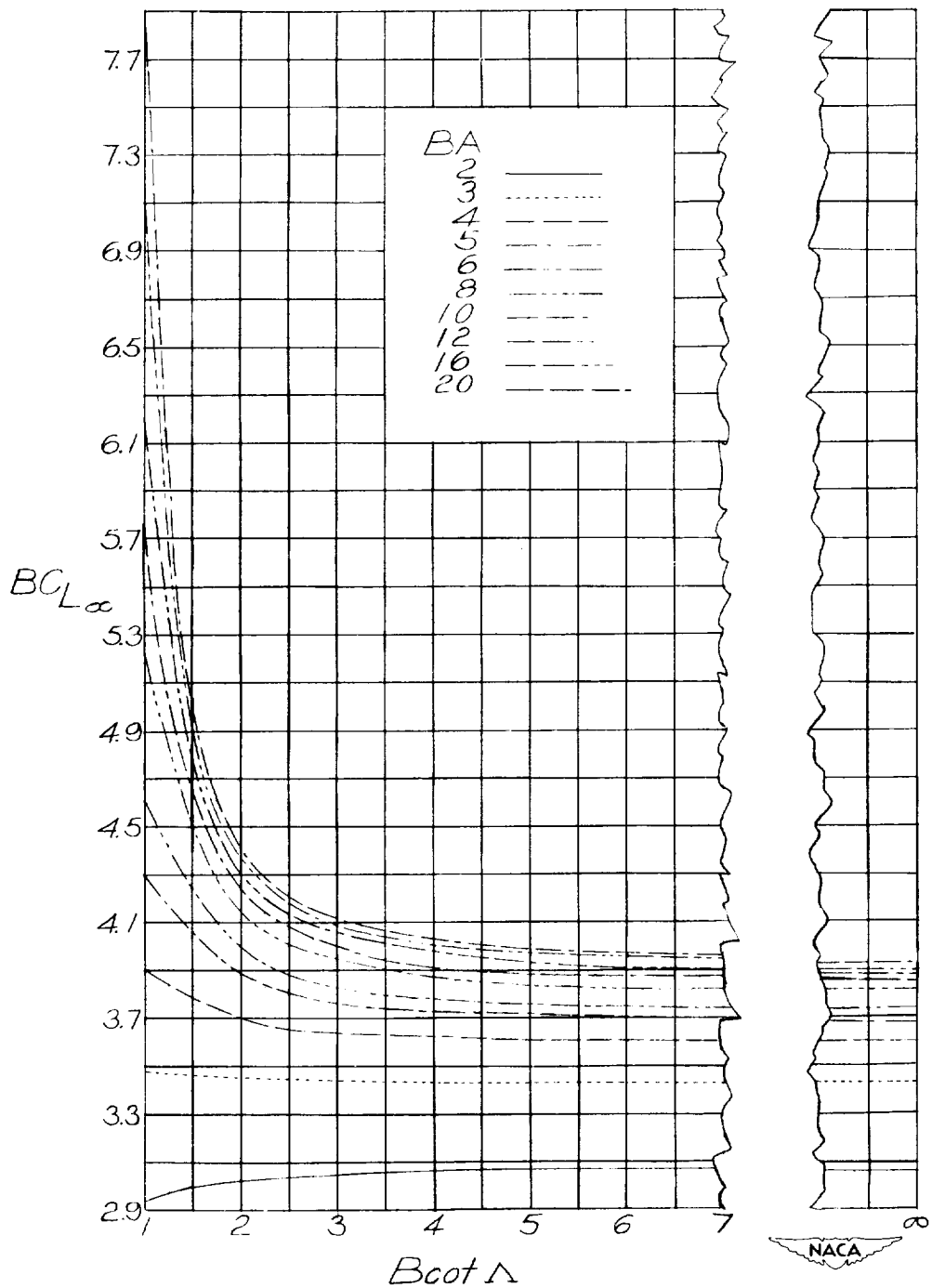

(d) Taper ratio $\lambda = 0.75$.

Figure 7.- Continued.

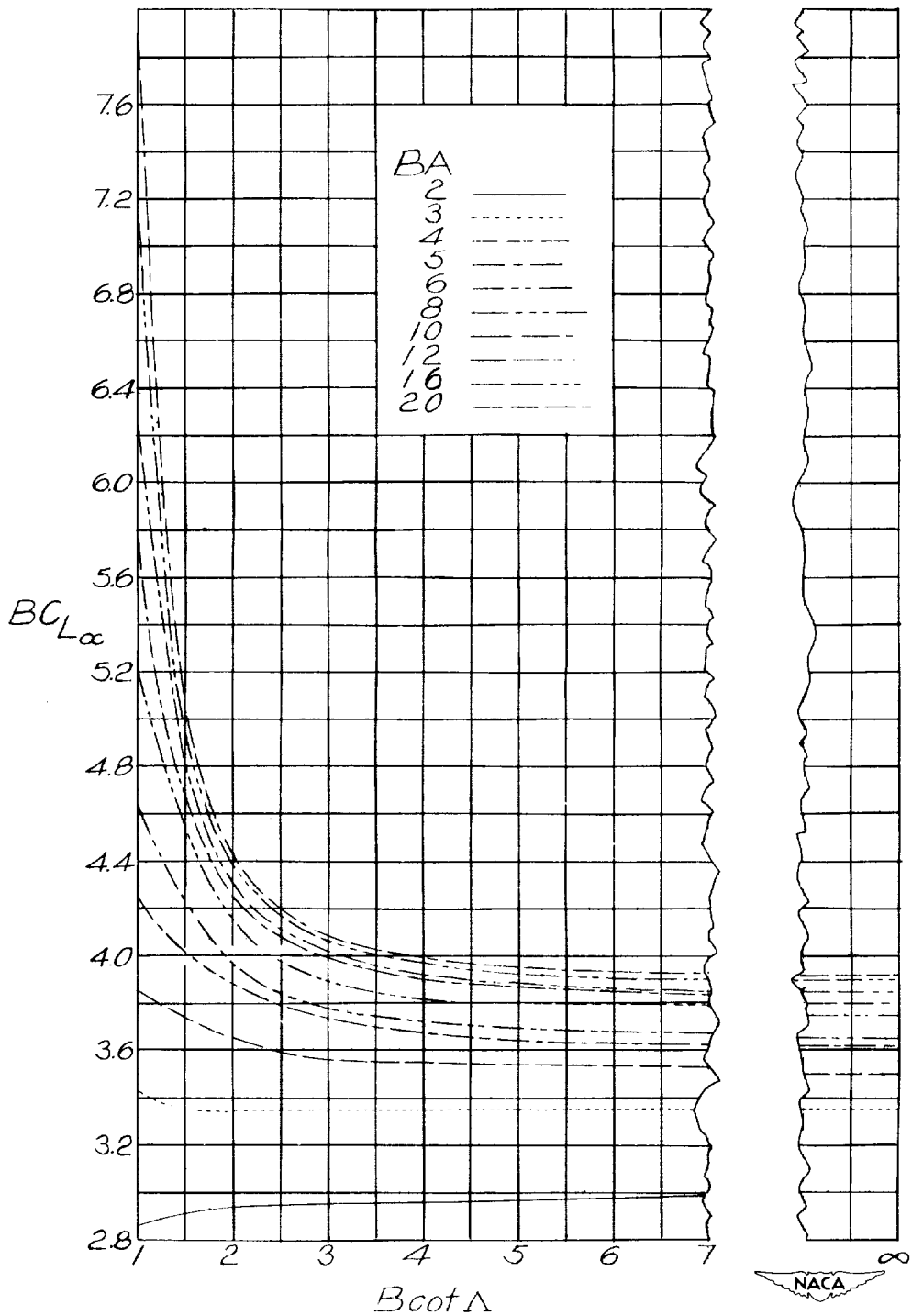

(e) Taper ratio $\lambda = 1.0$.

Figure 7.- Concluded.

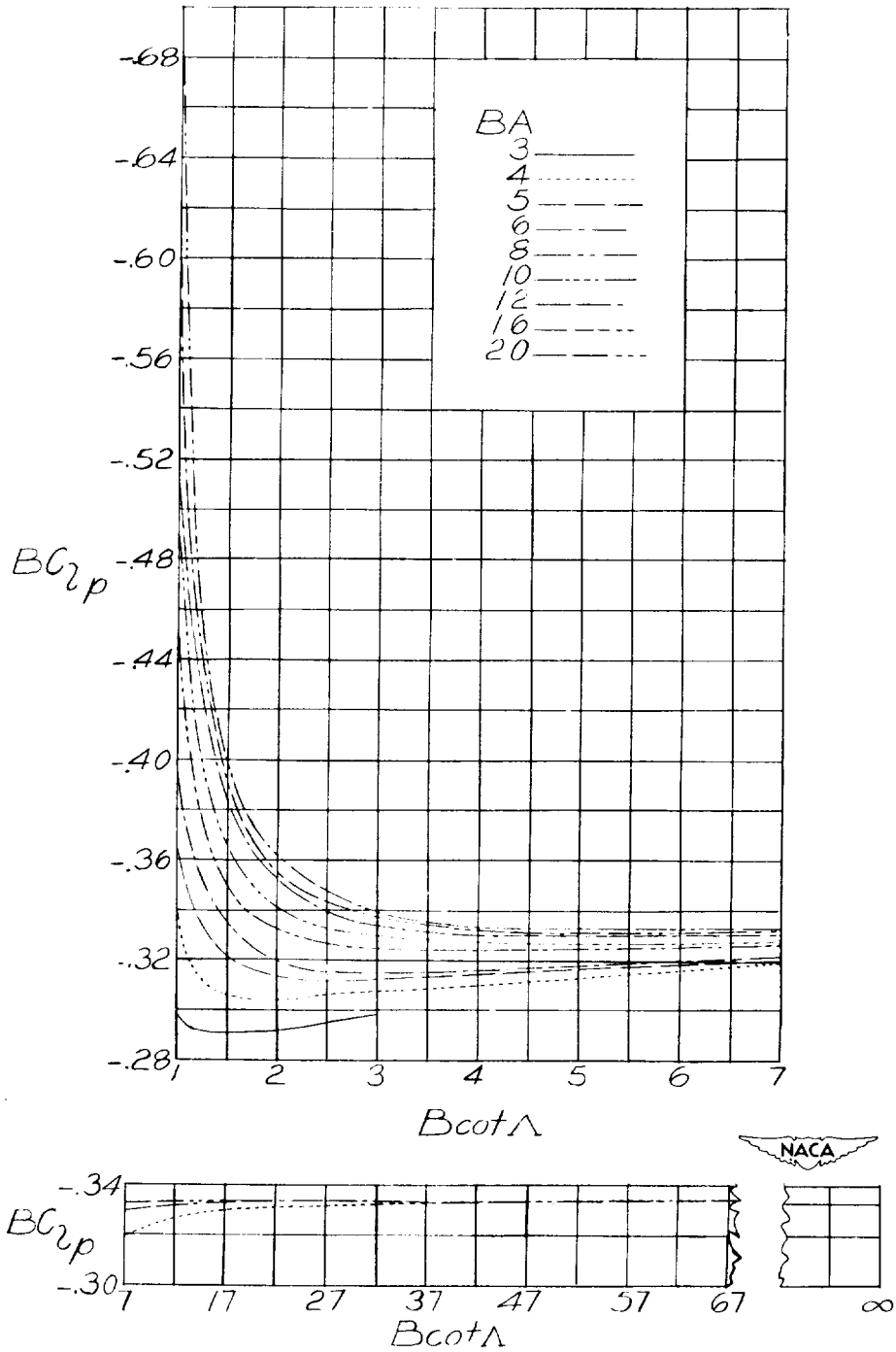

(a) Taper ratio $\lambda = 0$.

Figure 8.- Variation of BC_{l_p} with sweepback-angle parameter for various values of aspect-ratio parameter and taper ratio.

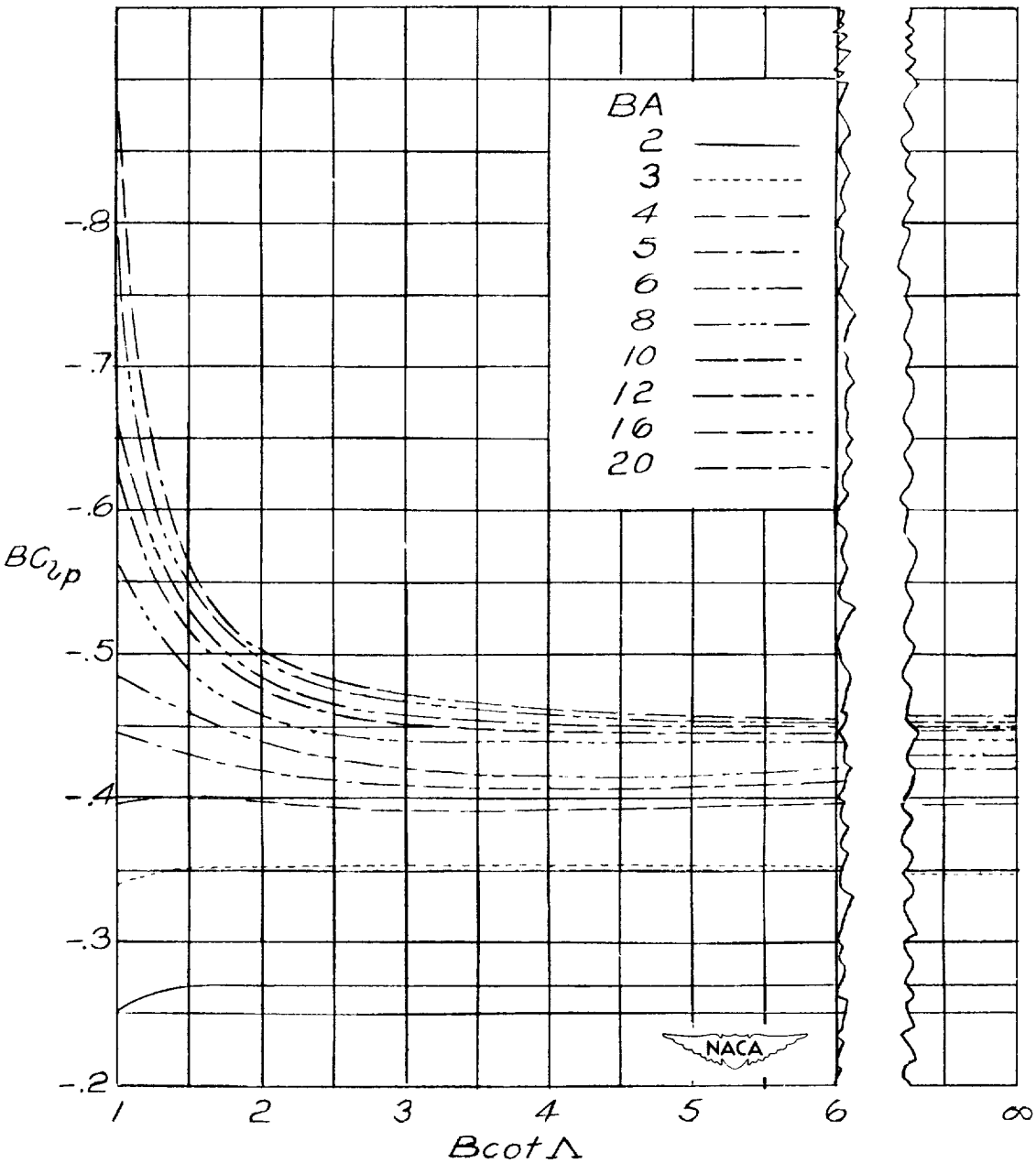

(b) Taper ratio $\lambda = 0.25$.

Figure 8.- Continued.

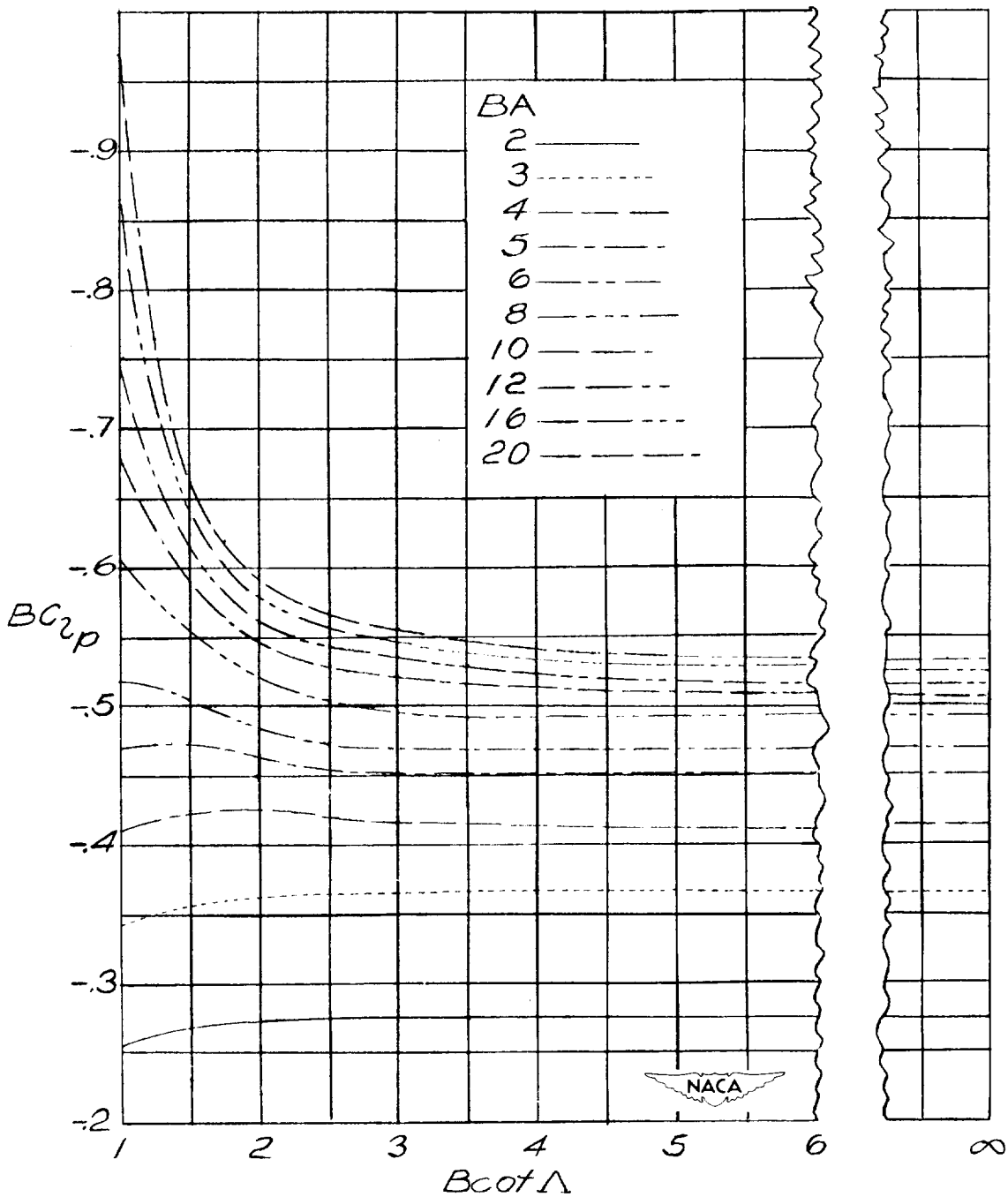

(c) Taper ratio $\lambda = 0.50$.

Figure 8.- Continued.

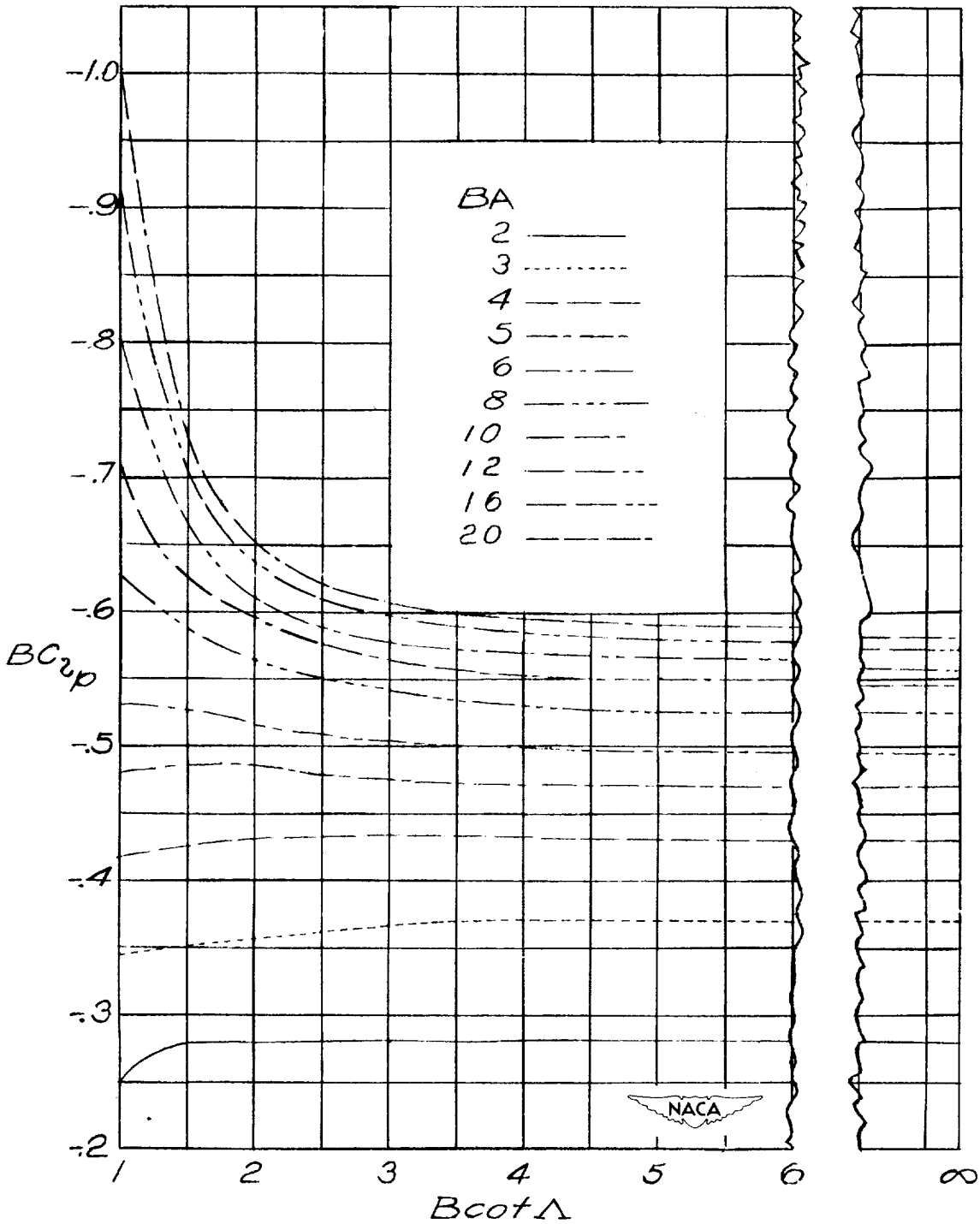

(d) Taper ratio $\lambda = 0.75$.

Figure 8.- Continued.

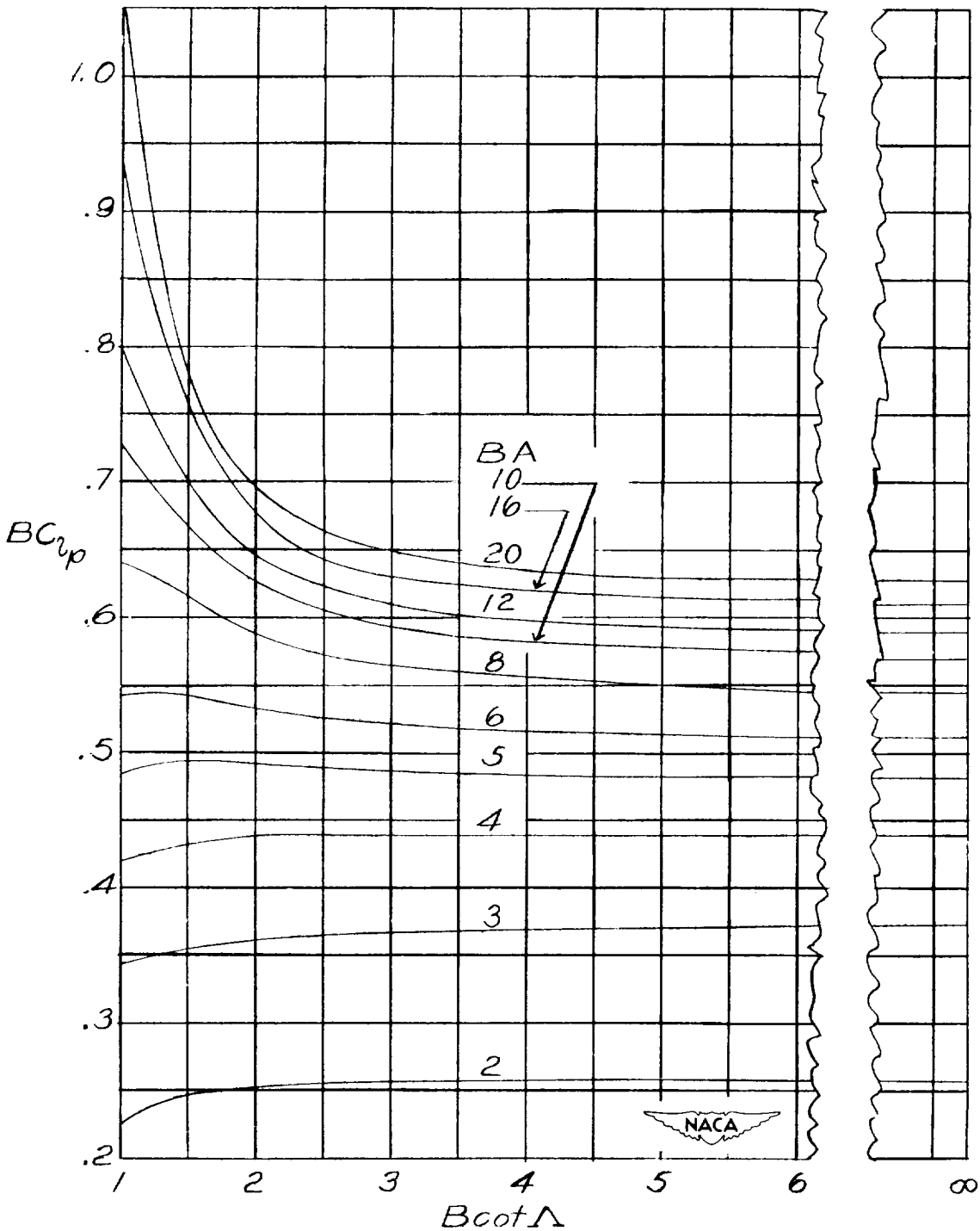

(e) Taper ratio $\lambda = 1.0$.

Figure 8.- Concluded.

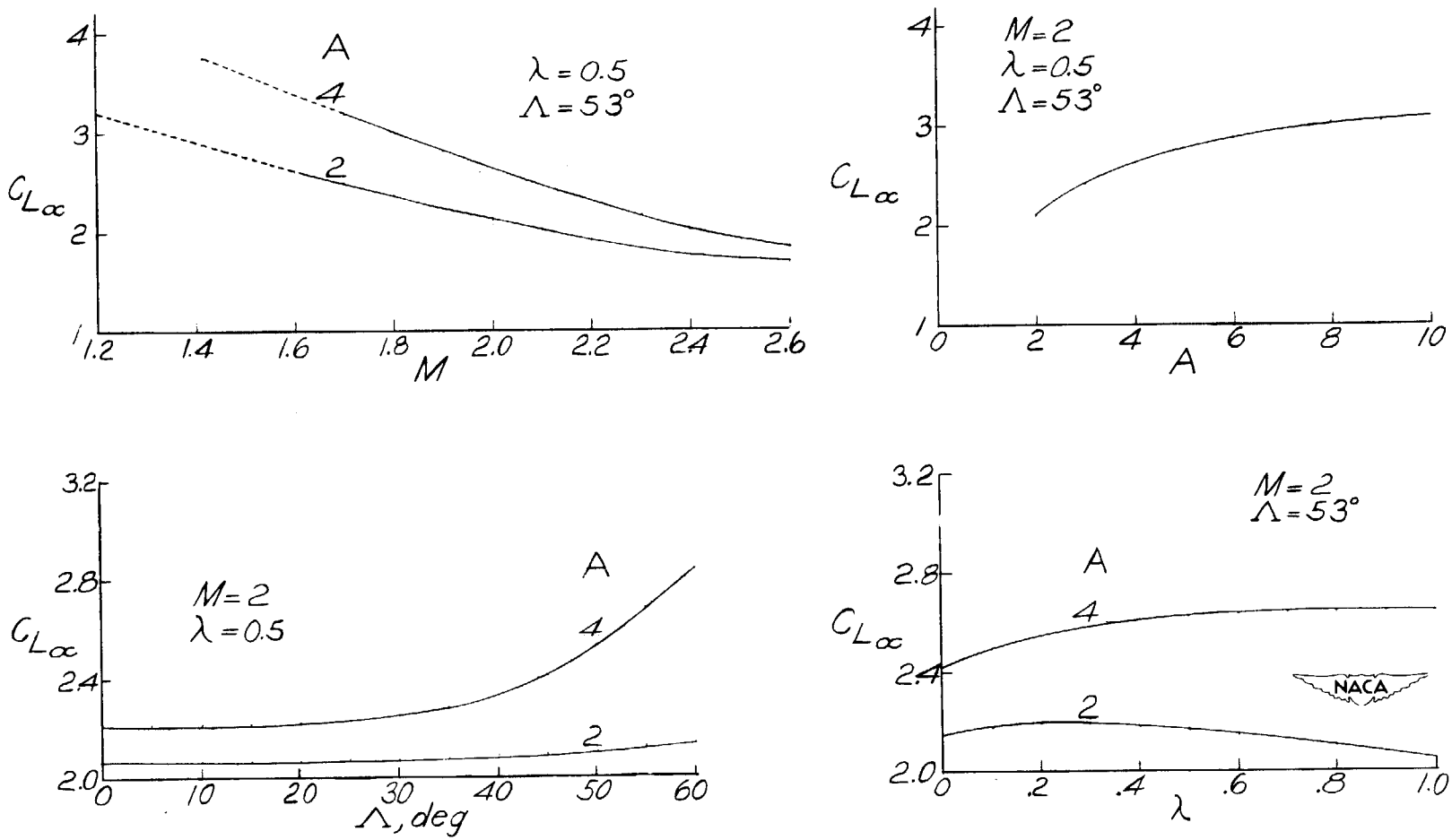

Figure 9.- Some illustrative variations of lift-curve slope C_{L_α} with Mach number, aspect ratio, sweep angle, and taper ratio. (Dashed portions of curves indicate subsonic leading edges.)

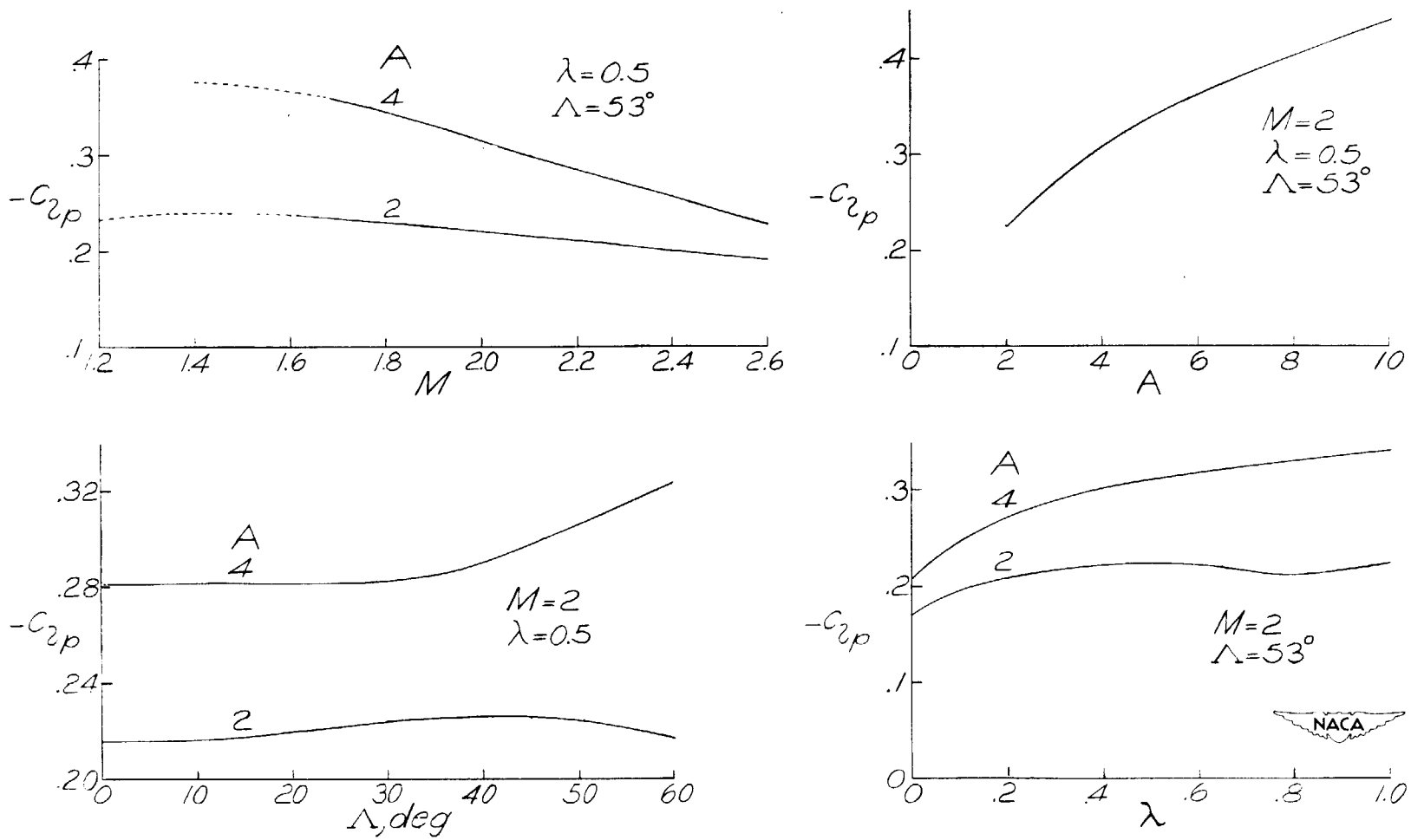

Figure 10.- Some illustrative variations of damping-in-roll derivative C_{l_p} with Mach number, aspect ratio, sweep angle, and taper ratio. (Dashed portions of curves indicate subsonic leading edges.)

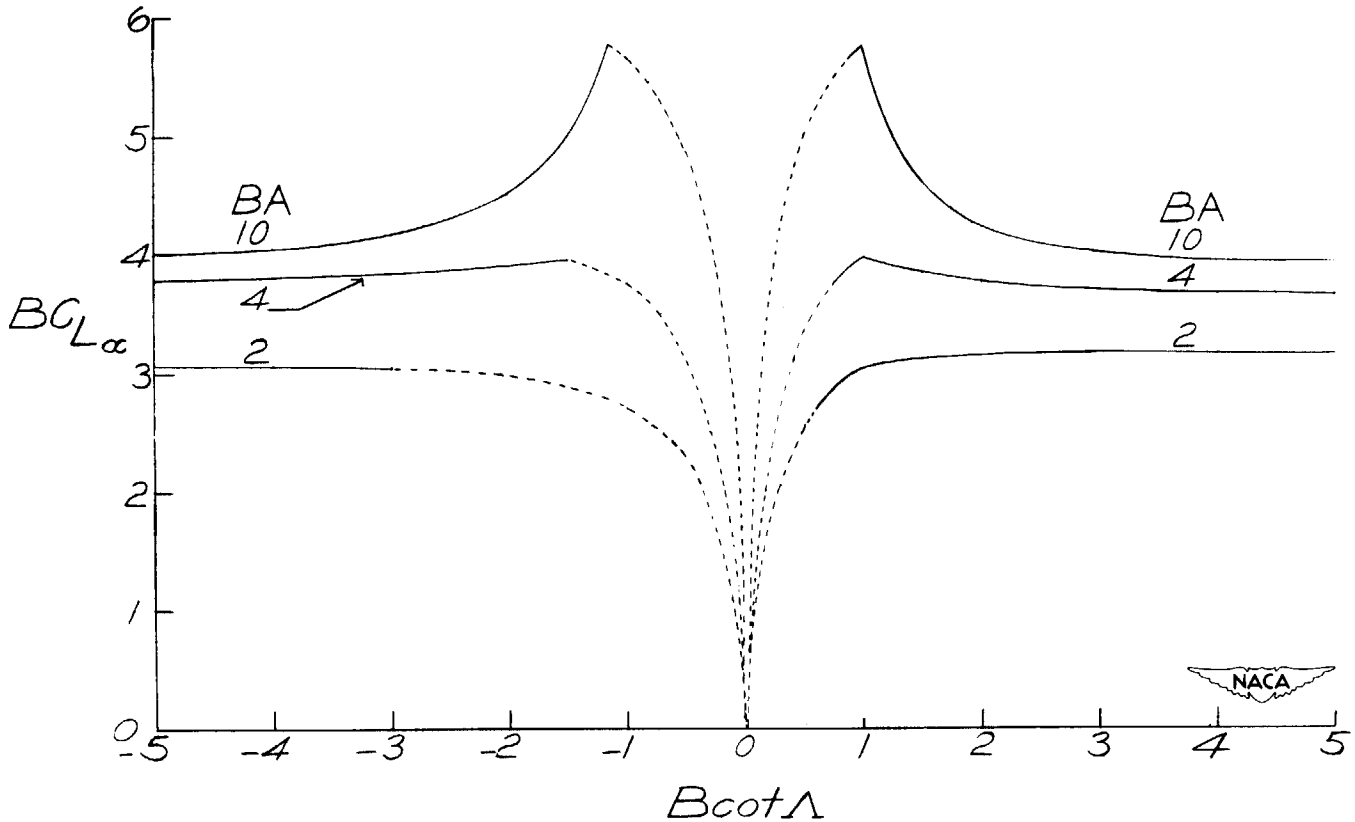

Figure 11.- Illustrative comparison of BC_{L_α} for sweptback and swept-forward wings for various values of aspect-ratio parameter. Taper ratio, 0.5. Dashed portions of curves refer to wings with subsonic trailing edges and have limited significance (see text).

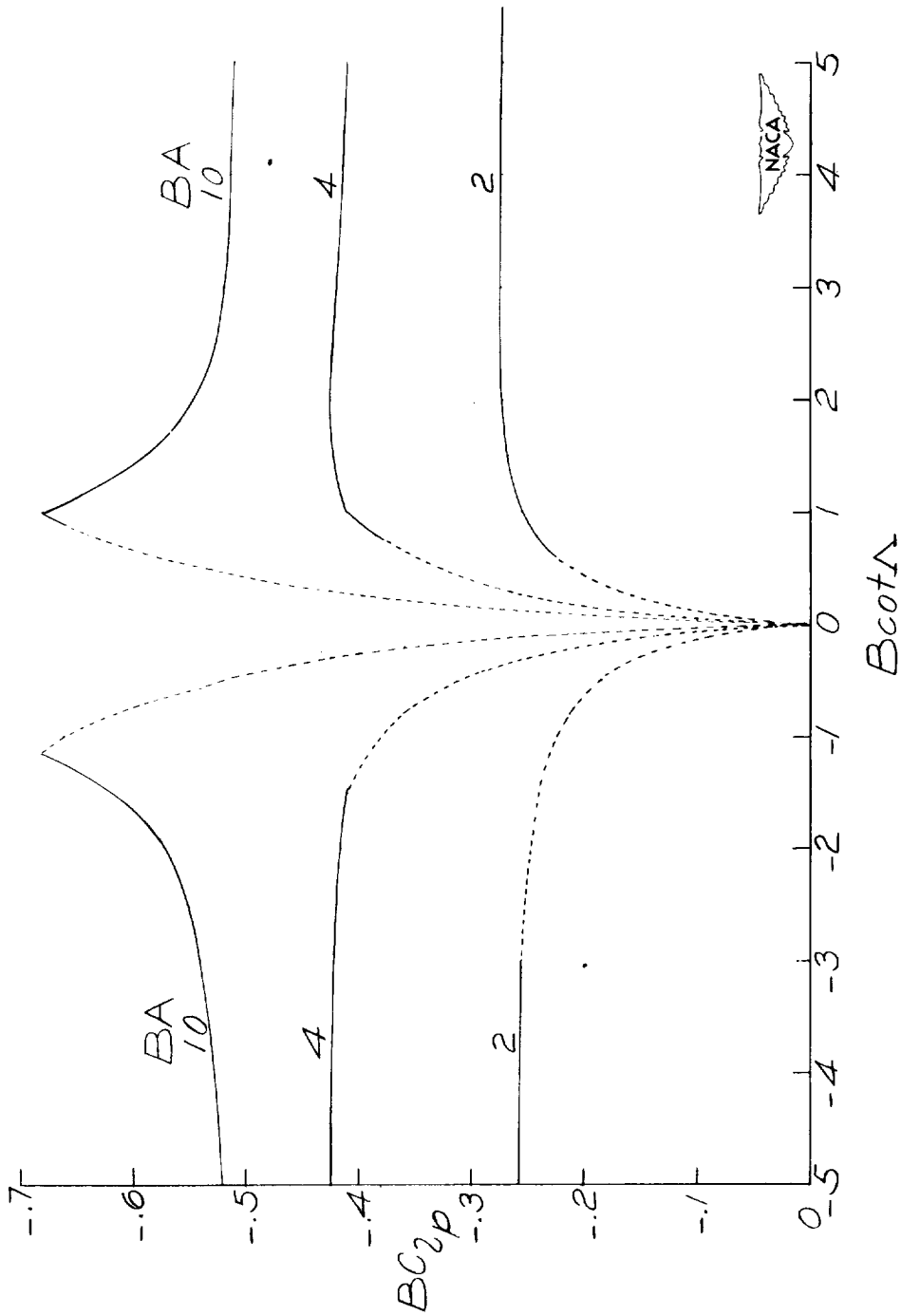

Figure 12.- Illustrative comparison of BC_{l_p} for sweptback and swept-forward wings for various values of aspect-ratio parameter. Taper ratio, 0.5. Dashed portions of curves refer to wings with subsonic trailing edges and have limited significance (see text).

NACA-Langley - 5-31-50 - 975